“Modeling and simulation of thermoelectric generators for use in industrial applications”

Thesis on

"Modeling and simulation of thermoelectric generators for use in industrial applications"

Jadavpur University

Department of Chemical Engineering

Submitted by

SOURODIP GHOSHDASTIDAR

Class Roll no.- 001710302006

Exam. Roll No.- M4CHE19005

Registration No.- 115778 of 2011-2012

Session: 2017-2019

Master of Chemical Engineering

Project Supervisor:

Prof. Kajari Kargupta

This project report is submitted towards the completion of Master of Engineering degree in Chemical Engineering.

Acknowledgement

I would like express my gratitude for the help, cooperation and inspiration that I have received from my teachers, friends and well-wishers during this course. It is their kind help and untiring effort that has resulted in completion of this project.

I thank God Almighty for all His blessings.

I am highly obliged and grateful to my Project Coordinator Prof. Kajari Kargupta, for her excellent guidance, endless encouragement and cooperation extended to me, right from the time of onset of this task till its successful completion.

I am very grateful to Prof. Debashis Roy, Head of the Department, Chemical Engineering Department for all the necessary help I got during my project work.

I am also indebted to Jadavpur University, Dept. of Chemical Engineering for supporting me and giving me the opportunity to use the equipments to do my research.

My sincere appreciation also extends to all my colleagues and others (especially Mr Sayantanu Mandal), who have provided assistance at various occasions; however, it is not possible to list all of them in this limited space.

I would also like to extend my thanks to our Lab assistant Mr Ajay Prodhan who has helped me all throughout my work.

I am grateful to my parents who encouraged and supported me all through and helped me in all respect.

……..

Sourodip Ghoshdastidar

CERTIFICATION

This is to certify that Mr Sourodip Ghoshdastidar, final year Master of Chemical Engineering(M.ChE) examination student of Department of Chemical Engineering, Jadavpur University, Examination Roll No M4CHE19005, Regn No 115778 of 2011-2012 has completed the Project work titled, "**Modeling and simulation of thermoelectric generators for use in industrial applications**" under the guidance of **Prof Kajari Kargupta** during his Masters Curriculum. This work has not been reported earlier anywhere and can be approved for submission in partial fulfilment of the course work.

……..	……
Prof. Debashis Roy	Prof. Kajari Kargupta
Head of Department and Professor	Project Supervisor
Chemical Engineering Department	Professor, Chemical Engineering Department
Jadavpur University	Jadavpur University

SIGNATURE OF DEAN

Abstract

A COMSOL model has been developed for a commercial thermoelectric generator (SP 1848-27145), which takes into account Thomson effect, Variable Material Properties and coupling of Electric potential field and Heat conduction equations. The model parameters were first tuned using experimental generated by the experimental group of Polymer Engineering Laboratory, Chemical Engineering Department, Jadavpur University. Thereafter the model was used to generate data at other operating conditions and they agree well with the experimental data.

A COMSOL inbuilt PEM fuel cell model was tuned with experimental data from an in house fuel cell in the Polymer Engineering Laboratory, Chemical Engineering Department, Jadavpur University. The model generates satisfactory results when compared with experimental data after tuning.

The COMSOL thermoelectric generator model and the tuned fuel cell model was combined to produce a hybrid FC-TEG system in COMSOL to perform waste heat recovery. Thereafter, the feasibility and window of operating zone for the same was determined. The study has significance in power generation for remote applications.

CONTENTS

CHAPTER I

Introduction

Modeling and simulation of thermoelectric generators for use in industrial applications

1.1 Background

Energy use is an important parameter which has far reaching effects on the economic growth and environmental pollution of a region. Various energy statistics agencies report and show that both industrial activities and energy sectors (power stations, oil refineries, coke ovens, etc.) are the most energy intense sectors worldwide and, thus, are accountable for the release of huge quantities of waste heat to the environment via hot exhaust gases, cooling media and heat lost from hot equipment surfaces and heated products. Recuperating and reusing waste heat would provide an attractive prospect for a low-carbon and less costly energy resource. Besides, the worldwide energy demand will rise by almost 35% by 2030 compared with the 2005s level or by up to 95% minus the use of energy efficient technologies [1]. Energy efficiency has been improved to a large extent due to concerted efforts, but a significant quantity of energy is still lost in forms of gas, liquid and solid, which requires waste energy recovery. For all the above-mentioned reasons, it is necessary to recover waste heat via capturing and reusing for heating or generating electrical or mechanical power in industrial processes. That way, the process efficiency will be increased, less fuel will be consumed and therefore less carbon dioxide will be emitted. The high and intermediate temperature waste can be directly utilized by driving steam turbine and gas turbine to generate electricity, but there are still difficulties in the utilization of waste heat in low-temperature range [1]. Thermoelectricity (TE), which is directly generated electric energy from waste heat sources shows promising results in making vital contributions to reducing greenhouse gas emissions and providing cleaner forms of energy [2]. The Thermoelectric Generator (TEG) can be used to convert heat to electricity through the Seebeck effect.

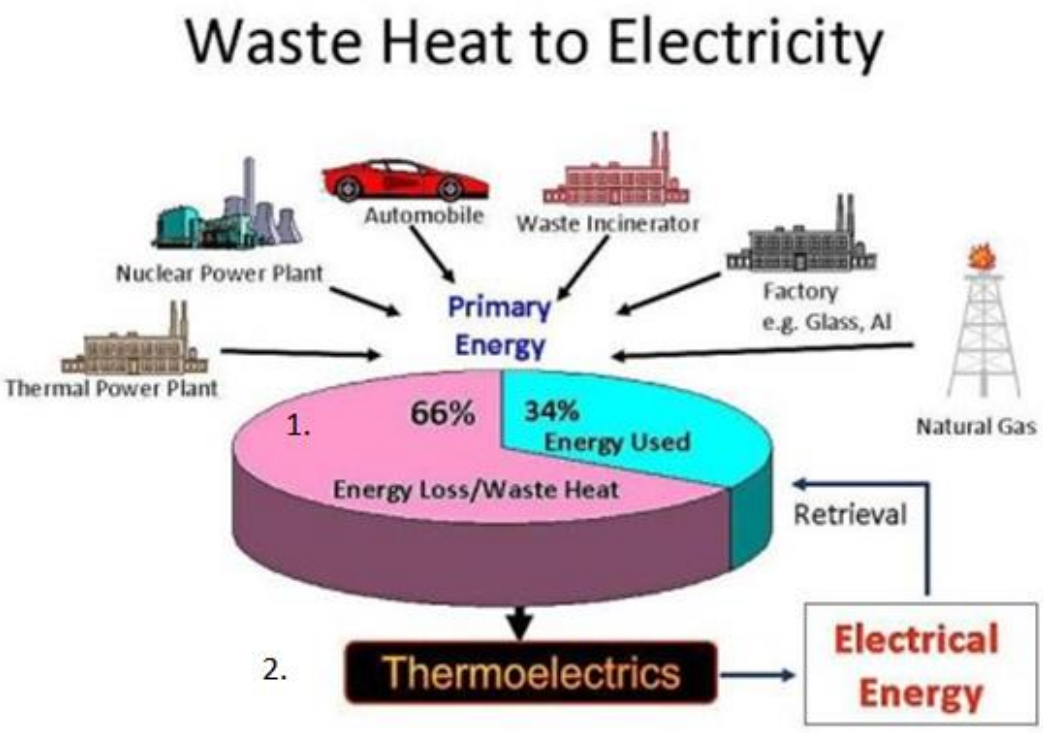

Fig 1.1 Diagram showing energy use, energy lost and energy retrieval using thermoelectrics(Ref [16])

1.2 Thermoelectric Generators(TEG)

A thermoelectric module(couple) is a solid state device consisting of a n-type and a p-type semiconductor and directly converts heat flux into electrical energy via the Seebeck effect. TEGs consist of a set of thermoelectric (TE) modules inserted between two heat exchangers. Each TE module is then composed of several tens to hundreds of pairs of TE couples connected together electrically in series and thermally in parallel, which directly convert a part of the thermal energy that passes through them into electricity. The advantages of TEGs are as follows:

1. Direct energy conversion, unlike many heat engines that first convert thermal energy into mechanical energy and then convert this mechanical energy into electricity using an alternator.
2. No moving parts and no working fluids inside the TEG, hence no maintenance and no extra costs.
3. A long lifespan, especially when working with constant heat sources.

4. Noiseless operations.
5. Emission free

Despite these advantages, for many years TEGs were limited to space applications where their extreme reliability justified their use to provide electricity to the majority of probes sent into space (Voyager, Apollo, Pioneer, Curiosity, etc.). Low efficiency and high cost have been a barrier to their development for more common applications

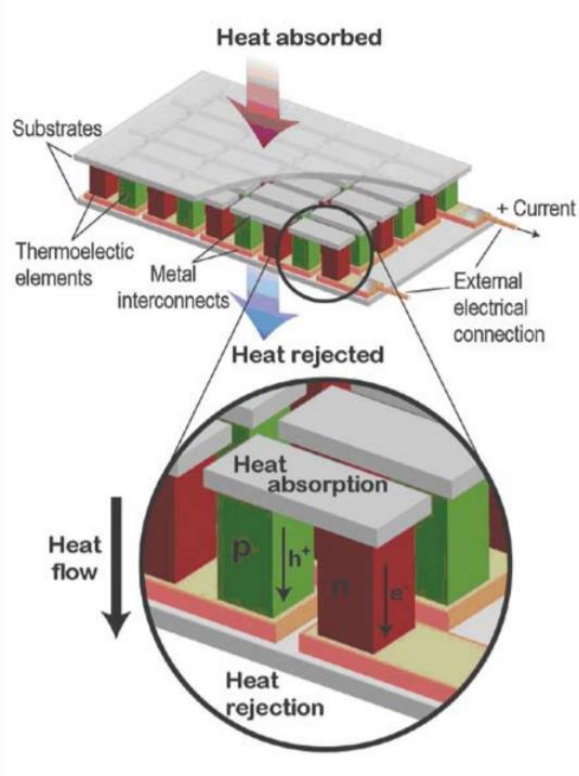

Fig 1.2 Thermoelectric Generator (Ref [15])

The application areas of thermoelectric generators are as follows:

1. Radioisotope thermoelectric generator(spacecraft)
2. Submarines
3. In remote areas, the use of TEGs can produce electricity reliably and with minimal maintenance.
4. Waste heat recovery from automobiles and aircraft.
5. Waste heat recovery from industries.

Challenges of thermoelectric generator deployment are as follows:

1. Low efficiency of conversion of heat to electricity
2. High material cost

Ongoing research serves to overcome these challenges. Composite materials are being developed in which scattering of phonons and electrons can be tuned independently to produce materials with high electrical conductivity and low thermal conductivity. Bio compatible conducting polymers are being developed which cost less than semiconductors and are less toxic.

1.3 Thermoelectricity

The term thermoelectricity refers to the phenomena in which a flux of electric charge is caused by a temperature gradient or the opposite in which a flux of heat is caused by an electric potential gradient. These phenomena include three effects; the Seebeck, Peltier and Thomson effect. The German physicist Thomas Johann Seebeck discovered the first of the thermoelectric effects in 1821. He found that a circuit made out of two dissimilar metals would deflect a compass needle if their junctions were kept at two different temperatures. Initially, he believed that this effect was due to magnetism induced by the temperature difference, but it was later discovered that it was due to an induced electric current. The second of the effects was observed by the French watchmaker Jean Charles Athanase Peltier in 1834. He discovered the heating or cooling effect occurring at a junction of two dissimilar metals when current is passed through it. The third effect was observed by the British physicist William Thomson (later Lord Kelvin) in 1856. He discovered that there is a heat exchange with the surroundings when there is both a temperature gradient and a flow of electric current in a conductor, in addition to the Joule heating. He also acknowledged the dependency between the Peltier and Seebeck effects, and by applying the theory of thermodynamics he established a relationship between the coefficients that describes the Peltier and Seebeck effects. These relations are known as the Kelvin relations. However, there was a slow progress in the field of thermoelectricity. Applications of the thermoelectric effects were limited to temperature measurements. New interest into the field came with the discovery of semiconductors in the 1930s. The introduction of semiconductors as thermoelectric materials in the 1950s made it possible to make Peltier refrigerators and thermoelectric generators with sufficient efficiency for special applications the interest in thermoelectricity waned until new interest was shown in the beginning of the 1990s.

1.4 Thermoeletric devices

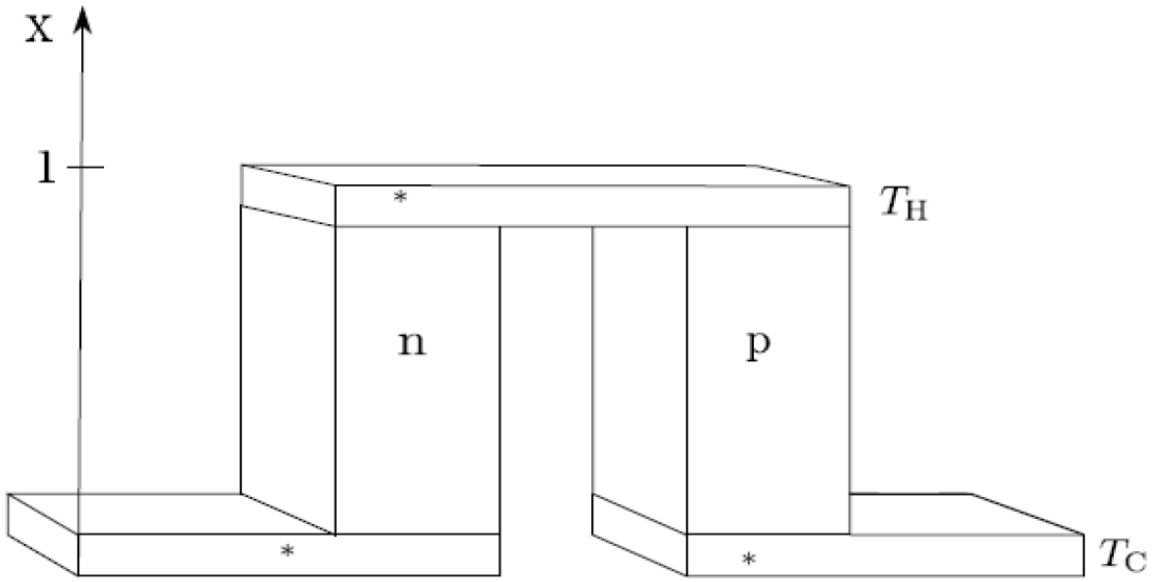

Fig 1.3 The basic unit of a thermoelectric device

A pair of n- and p-type semiconductors, known as a thermocouple, is the constitutive unit of a thermoelectric module [3]. A schematic drawing of the basic unit is shown in figure 1.3. The n-type and p-type semiconductors are connected electrically at one end. The electric conductors are marked by * in the figure. TH and TC are the hot side temperature and cold side temperature, respectively. The representative semiconductor pair geometry is as shown in figure 1.3 and the semiconductor sizes is normally in the order of millimetres. A thermoelectric device converts thermal energy to electrical energy by using an array of thermocouples. This device is a consistent source of power for satellites, space probes, and even unmanned facilities. In the figure 1.4, Electrons on the hot side of a material are more energized than on the cold side. These electrons will flow from the hot side to the cold side. If a complete circuit can be made, electricity will flow constantly. The electrons flow from hot to cold in the “n type,” while the holes flow from hot to cold in the “p type.” This allows them to be united electrically in series. To increase voltage and power output, elements are joined in series

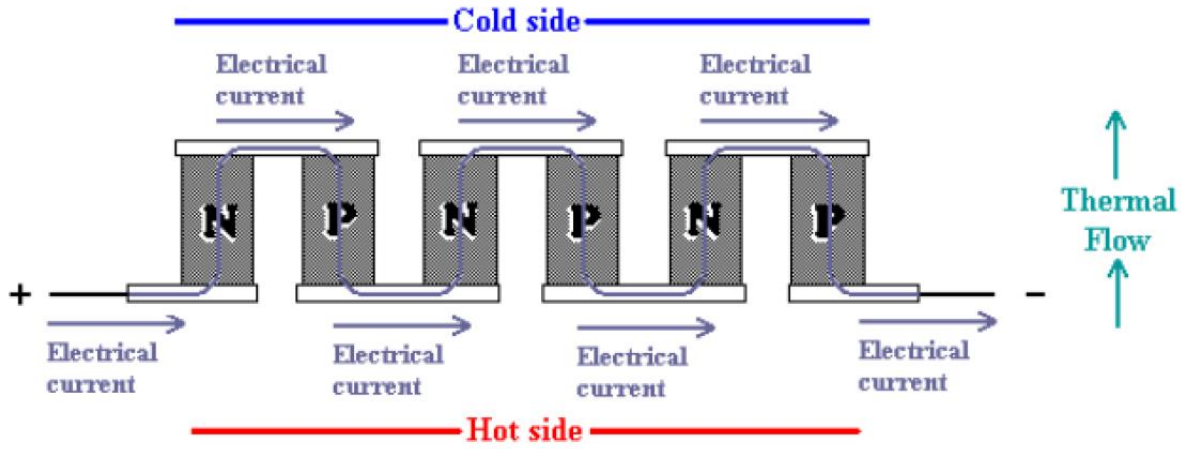

Fig 1.4 Diagram showing the heat and current flows in a TEG

1.5 Thermoelectric materials: choice of Bismuth Telluride as a thermoelectric material

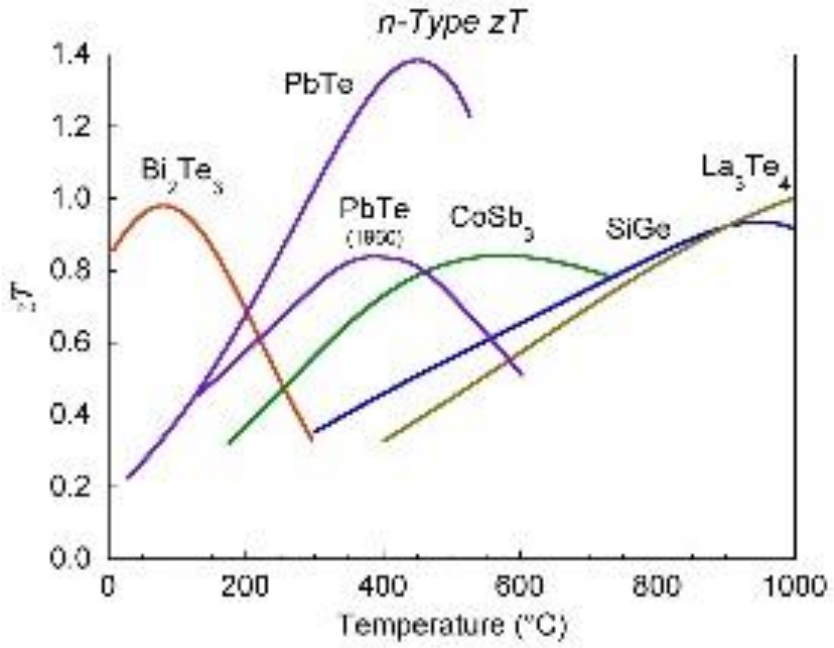

Fig 1.5 Plot of figure of merit of various thermoelectric materials against temperature(Ref [17])

Thermoelectric performance of Bi2Te3-based thermoelectric materials in the temperature range of 200 K to 500 K (including n type and p type; modified by doping) in the field of semiconductor alloys is the best [4], since it has the the highest value of ZT(figure of merit) in the given temperature range, which is why it has been selected for use in our models.

1.6 Working Principle of a Thermoelectric Generator

1.6.1 Seebeck effect

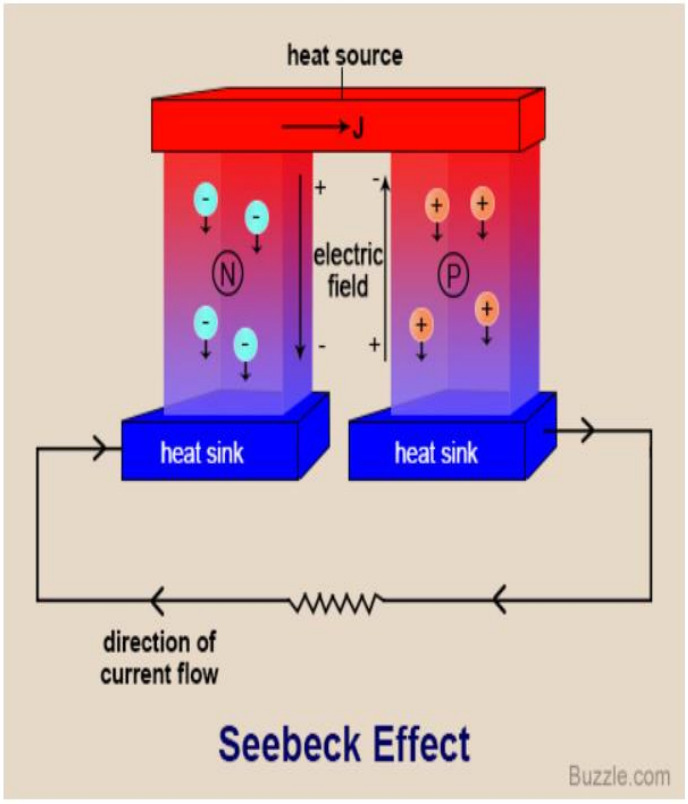

Fig 1.6 Seebeck Effect (Ref [18])

The Seebeck effect was found by Thomas Seebeck in 1821. He found a direct current flows in a closed electric circuit with two different materials maintained at different temperatures.

Electrons(holes) at the 'hot' end of the n-type(p-type) conductor receive the thermal energy from the source. They get energized and flow towards the 'cold' end. Distribution of charges builds an electric field across the junction. When a conductor is used to connect the two ends of the junction, charges begin to flow through it, and electric current is produced.

The open circuit potential difference in the circuit whose junctions are maintained at temperatures Th and Tc is given by $\Delta V = S_{AB}(Th-Tc)$. This is known as the Seebeck effect.

Semiconductors are the preferred type of thermoelectric material due to low thermal conductivity, high electrical conductivity, and high Seebeck coefficient.

1.6.2 Peltier effect

The Peltier effect is the phenomenon that a potential difference applied across a thermocouple causes a temperature difference between the junctions of the different materials in the thermocouple.

Heat absorbed at cold side: directly proportional to the current flowing in the circuit, the temperature of the cold side and the Seebeck Coefficient.

Heat rejected at hot side: directly proportional to the current flowing in the circuit, the temperature of the hot side and the Seebeck Coefficient.

Two counteracting Phenomena-Joule heating and thermal conduction. The net cooling power is the Peltier cooling minus these two effects

.

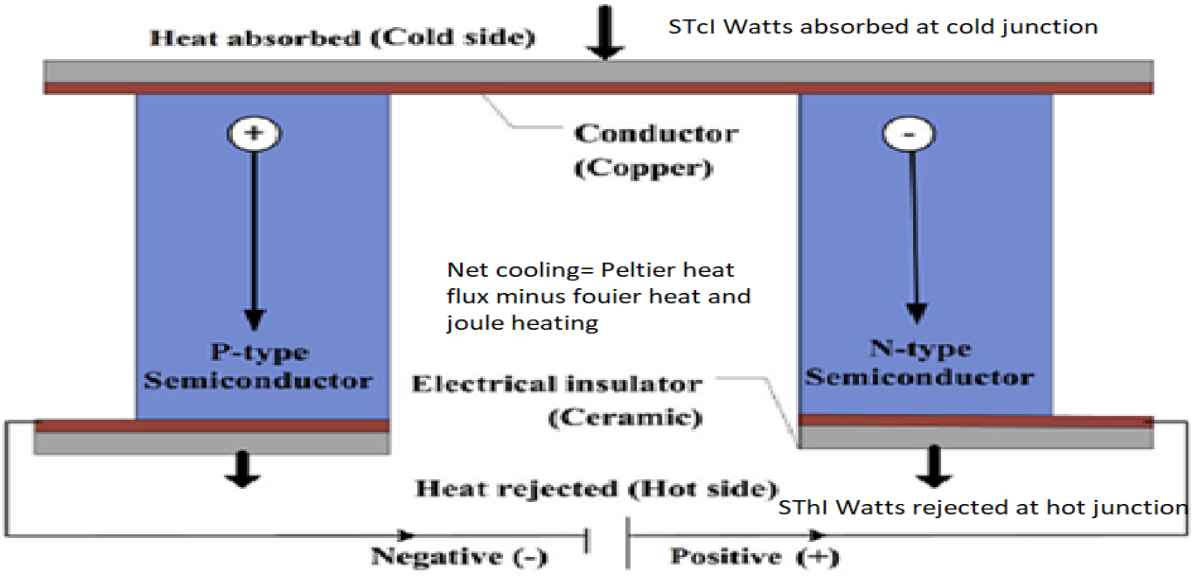

`

Fig 1.7 Peltier Effect

1.6.3 Thomson effect

Thomson effect describes the dissipation or absorption of heat, when electric current passes through a circuit composed of a single material, which has temperature variation along its length,. ΔQ represents heat dissipation, when electrical current flows through a homogeneous conductor. Thomson coefficient is given by second Kelvin relationship

$$\beta = T\frac{d\alpha}{dT}$$

where β and T, respectively, symbolize Thomson coefficient and temperature. If Seebeck coefficient, α, is temperature independent, then Thomson coefficient is equal to zero.

1.6.4 Figure of merit

$$ZT = \frac{\alpha^2 \sigma T}{K}$$

The definition of ZT shows that a material with large Seebeck coefficient (to generate high output voltage), low thermal conductivity (to maintain the temperature difference) and low electrical resistance (to reduce joule heating) has better performance in thermoelectric.

1.7 Fuel Cell-Thermoelectric Generator hybrid

For portable application purpose and for smart grid use, a hybrid device based on waste heat utilization was conceptualized. This hybrid device consists of high temperature proton exchange membrane fuel cell stack, heat sink, thermoelectric generator, coolant devices, and a battery. The waste heat produced by the fuel cell would flow into the thermoelectric generator, which would perform waste heat recovery from it. The fuel cell system is completely self-sustained and would not rely on any parasitic power to operate the internal heater. This will make the hybrid system a completely independent power generating source and can be used for any remote applications like power generation in mountain, desert, seacoast, battlefield which has limited access to utility grid. The continuous power will be provided by fuel cell, whereas the surplus power will be provided by TEG.

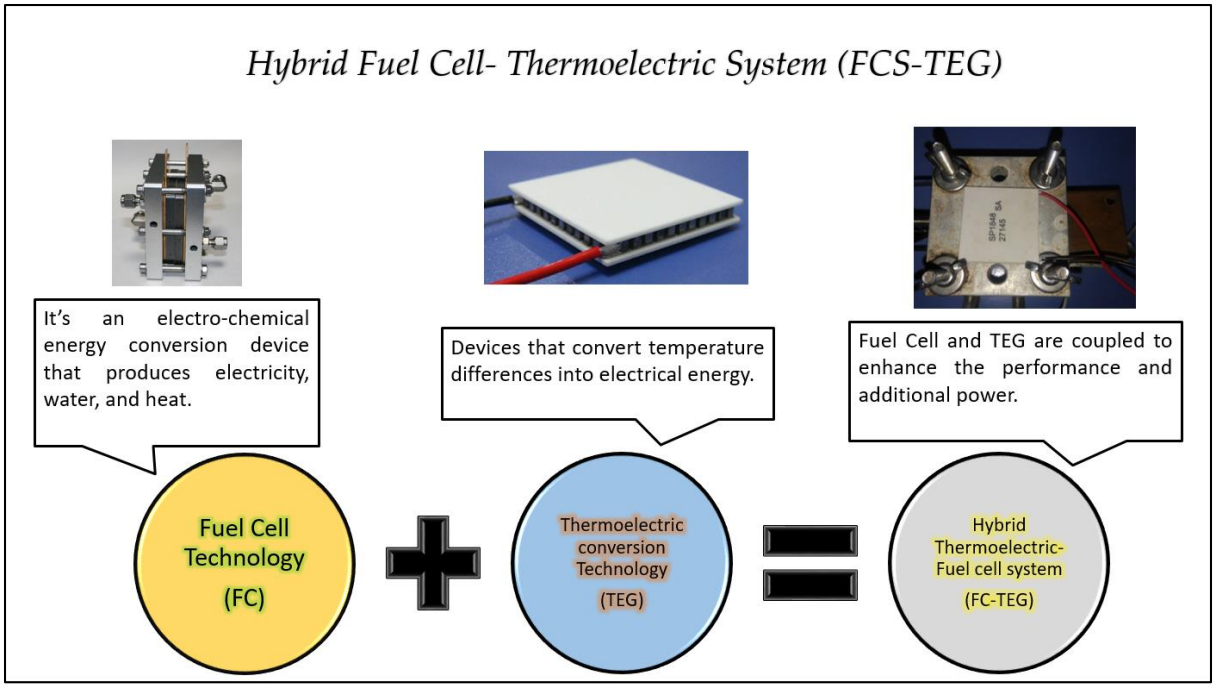

Fig 1.8 Hybrid Fuel Cell-Thermoelectric generator system

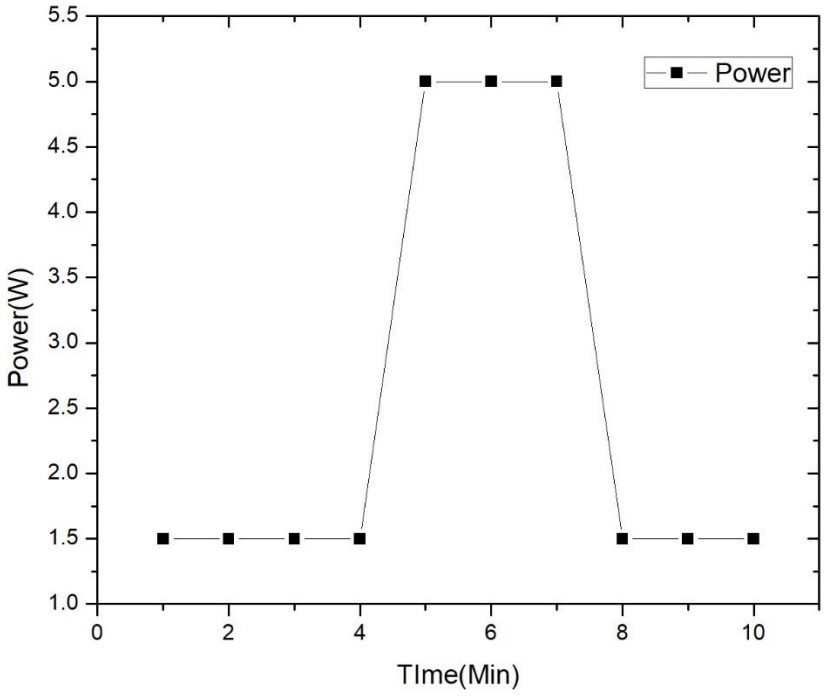

Fig 1.9 The continuous power provided by fuel cell, whereas the surplus power will be provided by TEG.

1.8 Fuel cell

Fuel cells produce electricity by an electrochemical reaction. In this reaction, oxygen and a hydrogen-rich fuel combine to form water. Fuel cells release energy electrocatalutically, as compared to internal combustion engines, which combusts fuel. The energy efficiency of fuel cells stems from this fact. Both batteries and fuel cells convert chemical potential energy into electrical energy and also, as a by-product of this process, into heat energy. A battery, as compared to fuel cells, holds a definite amount of energy. When this is depleted, the battery must be either discarded or recharged. A fuel cell, on the other hand, uses an external supply of chemical energy and can run indefinitely, as long as it is supplied with a source of hydrogen and a source of oxygen (usually air).

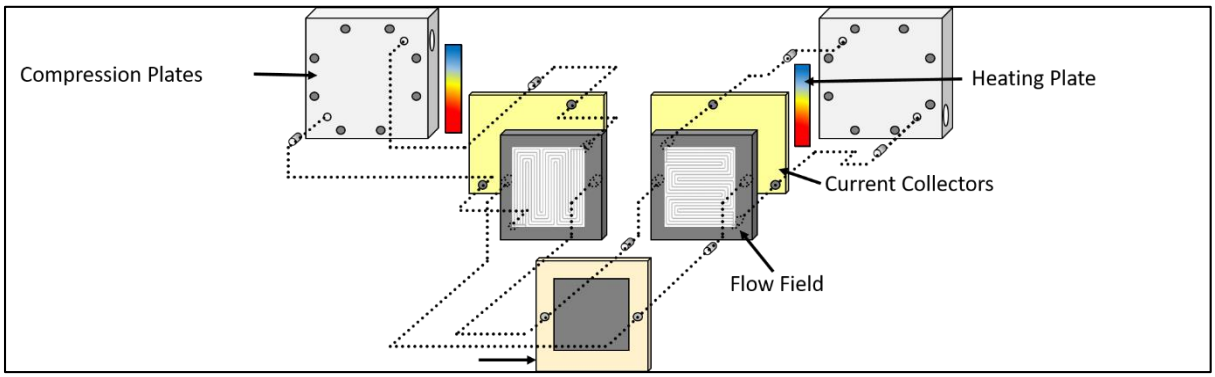

Fig 1.10 Parts of a fuel cell

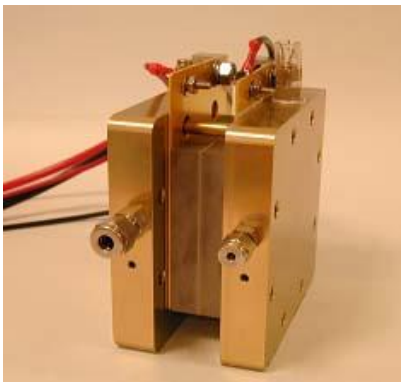

Fig 1.11 A single fuel cell

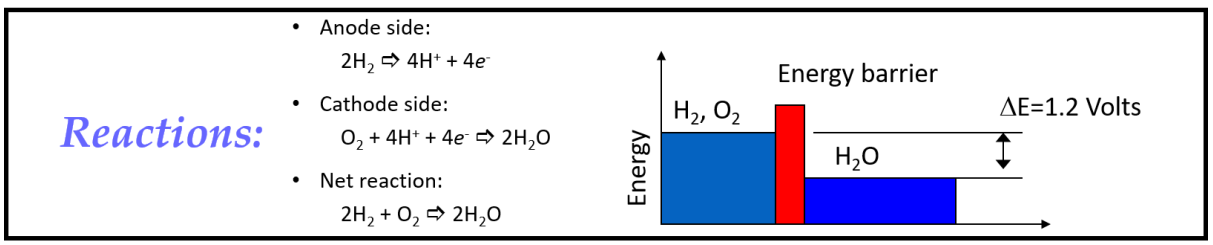

Fig 1.12 Electrochemical Reactions occurring inside a fuel cell

1.8.1 PEM Fuel Cells

Proton Exchange Membrane (PEM) fuel cells work with a thin permeable sheet known as a polymer electrolyte. Efficiency is around 45 percent, and operating temperature is about 80-160 degrees C. Power outputs are typically in the kW range. Leaking or cracking will not take place, due to the electrolyte being solid and flexible. Purification of fuels must be done, in addition to there being a platinum catalyst on both sides of the membrane, raising costs.

CHAPTER II

Aim and objective of the project work

Aim and objective of the project work

2.1 Aims and Objectives

1. Modeling of a single thermoelectric module in COMSOL and validation with data available in literature.
2. Modeling of a commercial thermoelectric generator (comprising of multiple thermoelectric couples) in COMSOL and validation with experimental data.
3. Tuning of an inbuilt PEM fuel cell model in COMSOL with experimental data.
4. Combining the fuel cell and thermoelectric generator model to form a hybrid Fuel Cell-Thermoelectric generator system to perform waste heat recovery.

CHAPTER III

Literature review

3.1 Literature Review

JOURNAL TITLE	JOURNAL NAME	AUTHOR NAME	DESCRIPTION
1. A three-dimensional numerical modeling of thermoelectric device with consideration of coupling of temperature field and electric potential field	Energy 47 (2012) 488-497	Xiao-Dong Wang Yu-Xian Huang , Chin-Hsiang Cheng, David Ta-Wei Lin, Chung-Hao Kang	A three-dimensional TE model with coupling of the temperature field and the electric potential field has been developed in this paper. All effect occurred in the TE are taken into account, such as the Joule heating, the Thomson effect, Fourier's heat conduction, the Peltier effect, the radiation and convection heat transfer, and temperature dependent properties of semiconductor materials.
2. Energy and exergy analysis of an annular thermoelectric cooler	Energy Conversion and Management 106 (2015) 804–814	S. Manikandan , S.C. Kaushik	The energy and exergy analyses of the annular thermoelectric cooler system considering Joule heating, Fourier Heat and Thomson effect have been carried out. It provides

			characteristics of the energy/exergy efficiency and the irreversibilities in an annular thermoelectric cooler system.
3. Characteristics analysis and parametric study of a thermoelectric generator by considering variable material properties and heat losses	International Journal of Heat and Mass Transfer 80 (2015) 227–235	Jing-Hui Meng , Xin-Xin Zhang , Xiao-Dong Wang	A three-dimensional and steady-state TEG model has been developed, which couples the temperature and electric potential equations and accounted for all thermoelectric effects, including the Seebeck effect, Peltier effect, Thomson effect, Joule heating and Fourier's heat conduction
4. Thermoelectric generators for waste heat harvesting: A computational and experimental approach	Energy Conversion and Management 148 (2017) 680–691	P. Aranguren , M. Araiz, D. Astrain, A. Martínez	The experimentation in this paper has been used to validate a general computational methodology which innovatively considers the temperature drop of the heat source as an essential parameter to simulate the thermoelectric generation of waste

			heat harvesting applications.
5. Study of the influence of heat exchangers' thermal resistances on a thermoelectric generation system	Energy 35 (2010) 602–610	D. Astrain, J.G. Vian, A. Martınez, A. Rodrıguez	A computational model capable of simulating the whole thermoelectric generation device, including the heat exchangers and the heat source, has been developed.
6. The study of a thermoelectric generator with various thermal conditions of exhaust gas from a diesel engine	International Journal of Heat and Mass Transfer 86 (2015) 667–680	Byung deok In, Hyung ik Kim, Jung wook Son, Ki hyung Lee b	This study measured the performance of thermoelectric modules in an actual engine system, using different heat sink shapes. In addition, the performance of a prototype thermoelectric generator is measured under various experimental conditions.
7. Waste heat recovery using a thermoelectric power generation system in a biomass gasifier	Applied Thermal Engineering 88 (2015) 274-279	Hsiao-Kang Ma, Ching-Po Lin, How-Ping Wu, Chun-Hao Peng, Chia-Cheng Hsu	This study analysed the gasification of waste biomass and the performance of a thermoelectric generation system, which is used to improve the use of

			waste heat in a downdraft gasifier.
8. Performance and Evaluation of a Fuel Cell–Thermoelectric Generator Hybrid System	FUEL CELLS 10, 2010, No. 6, 1164–1170	X. Chen, Y. Pan, J.Chen	The paper establishes a model of a hybrid system consisting of an SOFC, a regenerator and a thermoelectric generator. The optimally operating regions of the hybrid system, SOFC and thermoelectric generator are determined.
9. Numerical model of a thermoelectric generator with compact plate-fin heat exchanger for high temperature PEM fuel cell exhaust heat recovery	International Journal of Hydrogen Energy Volume 37, Issue 10, May 2012, Pages 8490-8498	Xin Gao, Søren Juhl Andreasen, Min Chen, Søren Knudsen Kær	A numerical model of a TEG heat recovery system for the exhaust gas from a HTPEMFC stack is developed. It is based on a finite-element approach with more precisely described gas properties and heat transfer.
10. Performance evaluation of an alkaline fuel cell/thermoelectric generator hybrid system	International Journal of Hydrogen Energy Volume 39, Issue 22, 24 July 2014, Pages 11756-11762	Puqing Yang, Ying Zhua Pei Zhang, Houcheng Zhang, Ziyang Hua Jinjie Zhang	An AFC-TEG hybrid system composed of an AFC, a multicouple TEG and a regenerator is established to effectively recover the waste heat released in the AFC.

CHAPTER-IV

Modeling of single thermoelectric element and a commercial thermoelectric generator

4.1 Numerical Model

In this section the numerical model of the thermoelectric generator is developed, with the equations solved in each domain of the thermoelectric generator detailed and discussed. In addition, the boundary conditions are detailed.

DOMAIN I	DOMAIN II	DOMAIN III
Heat Conduction Equation: $\nabla.(k\nabla T) = 0$ **Charge Conservation:** $\nabla.J = 0$ **Electric Potential Equation:** $\nabla.\left(\sigma(\nabla\emptyset)\right) = 0$ **I**	**Heat Conduction Equation:** $\nabla.(k\nabla T) + \frac{J^2}{\sigma} - \beta J.\nabla T = 0$ **Charge Conservation:** $\nabla.J = 0$ **Electric Potential Equation:** $\nabla.\left(\sigma(\nabla\emptyset - \alpha\nabla T)\right) = 0$ **II**	**Heat Conduction Equation:** $\nabla.(k\nabla T) = 0$ **Charge Conservation:** $\nabla.J = 0$ **Electric Potential Equation:** $\nabla.\left(\sigma(\nabla\emptyset)\right) = 0$ **III**

A **B** **C** **D**

Where $\beta = T\frac{d\alpha}{dT}$, the Thomson coefficient.

Subdomains I and III represent the heat source and heat sink respectively and subdomain II represents the thermoelectric material. (Refer fig 1.6)

The thermal boundary conditions are:

A: Temperature of the hot side Th is specified (T=Th, Dirichlet Boundary Condition).

B: The heat flux is continuous across the interface.

C: The heat flux is continuous across the interface.

D: Temperature of the cold side Tc is specified (T=Tc, Dirichlet Boundary Condition).

The electrical boundary conditions are:

A: Current flux is zero across the interface.

B: Current flux and potential is continuous across the interface.

C: Current flux and potential is continuous across the interface.

D. Current flux and potential at the first thermoelectric element is specified to be Jo (J=Jo, Dirichlet boundary condition) and zero (V=0, Dirichlet boundary condition) respectively, and for the rest of the thermoelectric elements, current flux is zero at the interface.

The total set of equations that have to be solved (the domains for which have been shown earlier) are as follows:

Heat Conduction Equation

$$\nabla.(k\nabla T) + \frac{J^2}{\sigma} - \beta J.\nabla T = 0 \qquad (4.1)$$

The first term consists of the divergence of the Fourier heat flow, the second term consists of Joule heating, and the third term signifies the Thomson effect. $\beta = T\frac{d\alpha}{dT}$, signifies the Thomson coefficient.

Charge Conservation

$$\nabla.J = 0 \qquad (4.2)$$

Electric Potential Equation

$$\nabla.\left(\sigma(\nabla\emptyset - \alpha\nabla T)\right) = 0 \qquad (4.3)$$

Where $\alpha\nabla T$ is the seebeck electromotive force.

Once the electric potential is obtained, the current density vector can be calculated by the following equation:

$$J = \sigma E = \sigma(-\nabla\emptyset + \alpha\nabla T) \qquad (4.4)$$

4.2 Material Properties(Ref [1])

Semiconductor:

K(thermal conductivity, (W K^{-1} m^{-1}): $0.000029T^2$-0.019593T+4.809677

ρ(electrical resistivity, Ωm): 10^{-6}(0.043542T-2.754139)

α, n-type(seebeck coefficient, (V K^{-1}): 10^{-6}(-$0.002025T^2$+1.423448T-44.953611)

α, p-type(seebeck coefficient, (V K^{-1}): -10^{-6}(-$0.002025T^2$+1.423448T-44.953611)

Connector(Cu)

K(thermal conductivity, (W K^{-1} m^{-1}): 350

ρ(electrical resistivity, Ωm): 1.695 X 10^{-9}

α(seebeck coefficient, (V K^{-1}): 6.5 X 10^{-6}

4.3 Case Study I: Validation of model with existing data available in literature (ref [7])

Geometry

The geometry of the thermoelectric modules has been developed according to the following information given in the paper, "A three-dimensional numerical modeling of thermoelectric device with consideration of coupling of temperature field and electric potential field" by Xiao-Dong Wang, Yu-Xian Huang, Chin-Hsiang Cheng, David Ta-Wei Lin, Chung-Hao Kang.

:

The geometric parameters and test grid numbers for TEC.

		L_1	L_2	L_3	H_1	H_2
Geometry	Value	0.1 mm	0.5 mm	0.2 mm	0.1 mm	1.0 mm
Grid i	Grid number	2	10	4	2	20
Grid ii	Grid number	4	20	8	4	40
Grid iii	Grid number	5	25	10	5	50
Grid iv	Grid number	6	30	12	6	60

Table 4.1 Geometric parameters for the thermoelectric module

Where L_1, L_2, L_3, H_1, H_2 are described as follows:

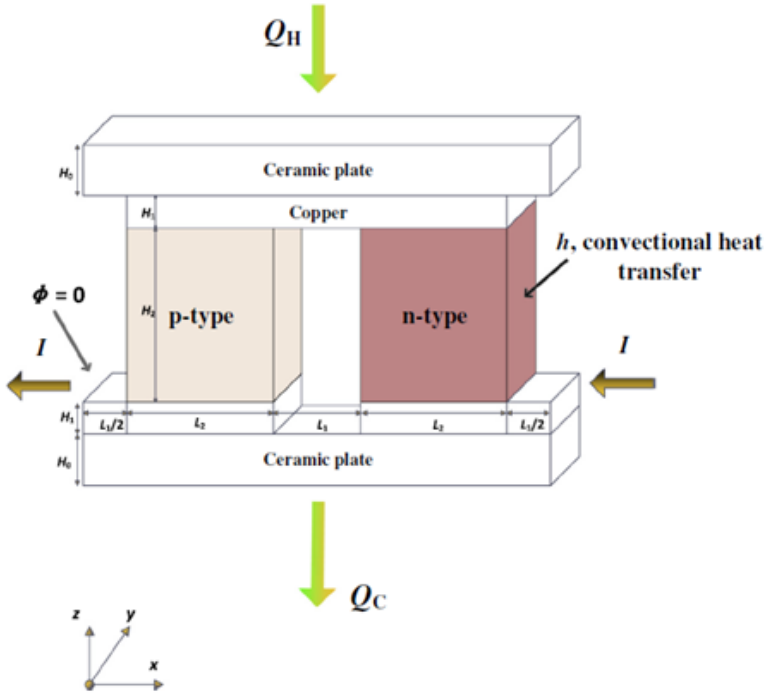

Fig 4.1 Geometry of the thermoelectric element which was validated (Ref [1])

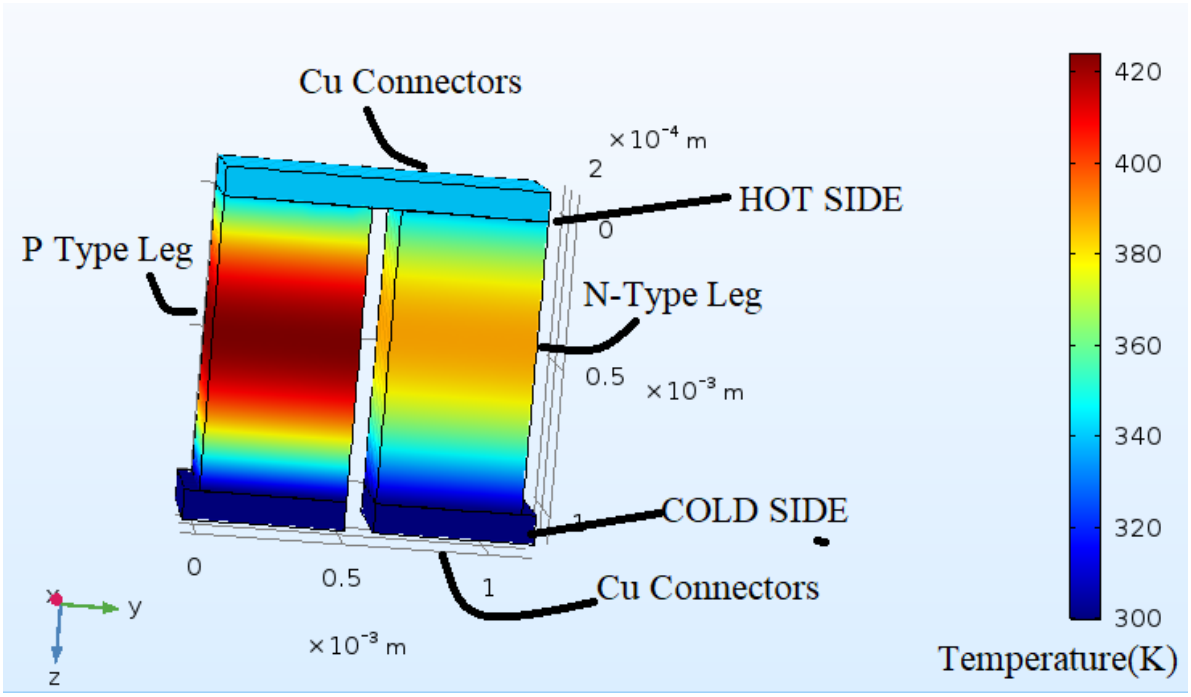

Fig 4.2 COMSOL Model

4.3.1 Boundary Conditions

Hot side temperature is kept at 340K.

Cold Side temperature is kept at 300K.

Input Current is 2.2A.

4.3.2 Methodology

The equations are solved simultaneously for each domain (I, II and III) for the thermoelectric module shown in Fig 4.2 in COMSOL 5.3. Here in the above figure, Domain I and III consists of the Cu connectors, while Domain II consists of the P-type and N-type legs. COMSOL uses the finite element method to solve the coupled heat equations and electric potential equations, and the results are obtained with input current =2.2A.

4.3.3 Results and Discussion

The temperature has been plotted as a function of length along the p type semiconductor leg:

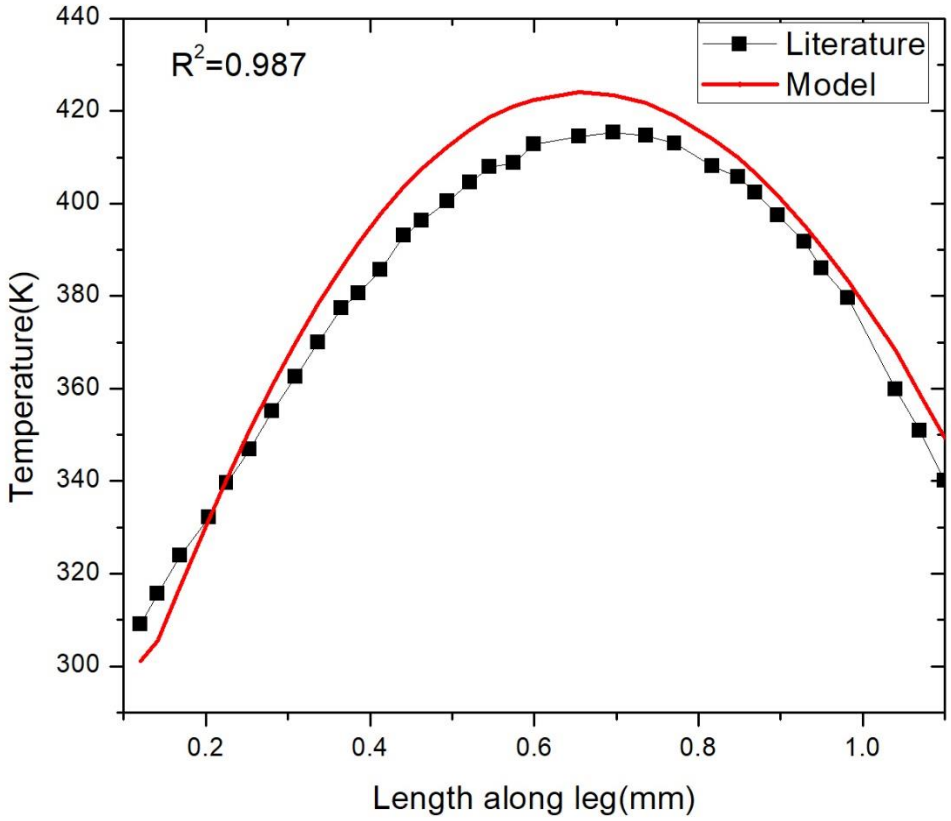

Fig 4.3 Temperature distribution of thermoelectric element along leg length

The temperature profile along the leg predicted by the COMSOL model agrees well with the data given in the literature. (Ref [1])

4.4 Case Study II: Estimation of design parameters of Commercial thermoelectric generator (SP 1848-27145)

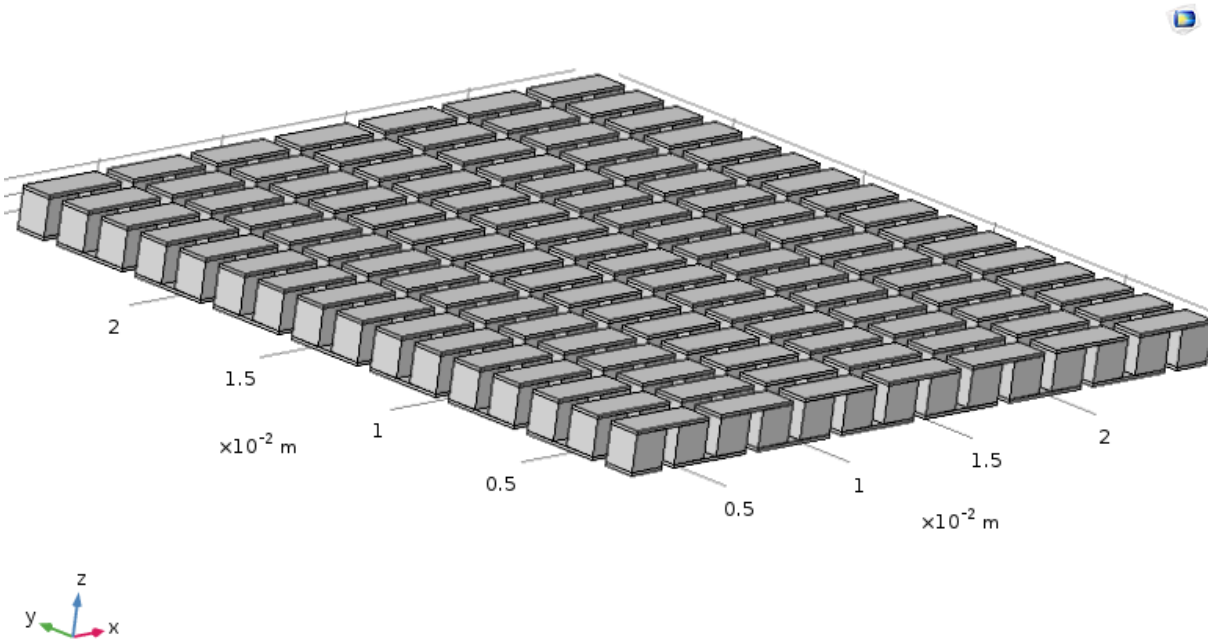

Fig 4.4 COMSOL model of the thermoelectric generator

Process Diagram

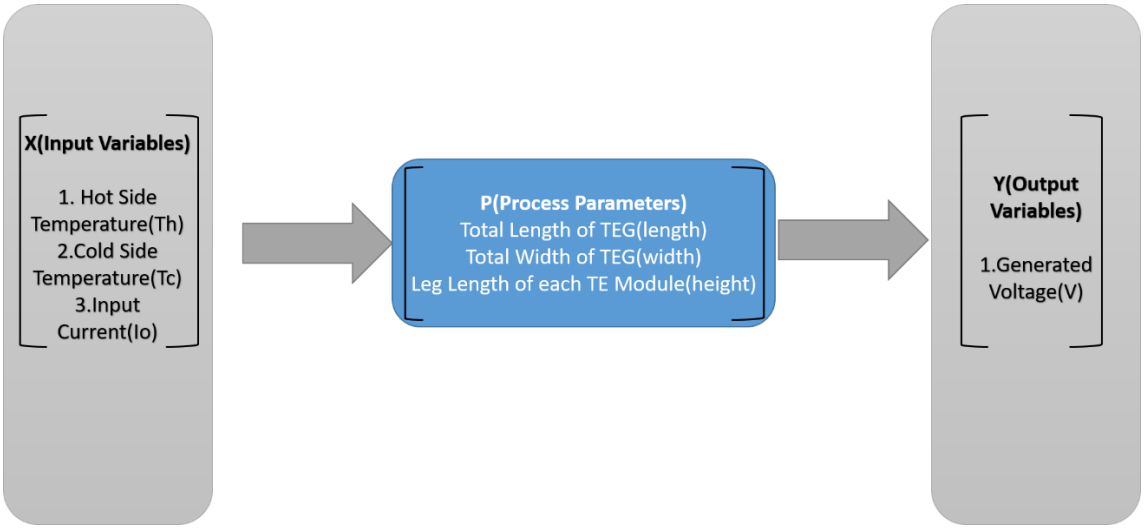

Fig 4.5 Process diagram of the thermoelectric generator, in which the input variables, output variables and the process parameters have been defined.

In this case study, a commercial thermoelectric generator (TEG) comprising of 112 thermoelectric elements in series are considered (Fig 4.4).

The input variables (X) and the output variables (Y) are known. However, the process parameters are unknown and are found out in this study. (Refer fig 4.5)

4.4.1 Methodology

The model parameters are tuned (Identification problem) to match with the experimental data generated by experimental group of Polymer Engineering Laboratory, Chemical Engineering Department, Jadavpur University.

The experimental Current-Voltage curve for the thermoelectric generator was generated at a temperature difference of 80K. The data for the same is as follows:

Table 4.2

Current (A)	Experimental Voltage(V)
0.1	1.915
0.2	1.915
0.3	1.752
0.4	1.423
0.5	1.125
0.6	0.875
0.7	0.569
0.8	0.369
0.9	0.112
1	0

The process parameters, which consist of the total width, total length, and individual leg length of every TE module, were tuned, so that the current voltage characteristics of the resultant geometry so formed agreed well with the experimental results shown above.

The values of the tuned parameters are shown in the table below:

Table 4.3

Parameter name	Parameter Value	Description
width	25.4[mm]	Total width
length	25.4[mm]	Total length
height	1.9075[mm]	Leg Height

4.4.2 Model Equations

Model equations are as shown in section 4.1 As in the previous case, the equations are solved simultaneously for each domain (I, II and III) for the thermoelectric generator shown in Fig 4.4 in COMSOL 5.3. Here in the figure 4.4 (COMSOL Geometry), Domain I and III consists of the Cu connectors, while Domain II consists of the P-type and N-type legs. COMSOL uses the finite element method to solve the coupled heat equations and electric potential equations.

4.4.3 Geometry

Geometry was formed in COMSOL from the tuned parameters in Table 4.3. The geometry is shown in fig 4.4.

4.4.4 Boundary conditions

Cold Side temperature of 293.15K

Hot Side Temperature of 373.15K

Input Current varying from 0.1A to 1A

4.4.5 Results and Discussions

The current voltage characteristics generated from the model, using the tuned parameters is shown in the table below:

Table 4.4

Current (A)	Experimental Voltage(V)	Voltage of tuned model(V)
0.1	1.915	2.4335
0.2	1.915	2.1235
0.3	1.752	1.8132
0.4	1.423	1.5026
0.5	1.125	1.1915
0.6	0.875	0.88004
0.7	0.569	0.56809
0.8	0.369	0.25564

The current voltage characteristics of the TEG are plotted (voltage plotted against current) and a comparison is made between the experimental data used for tuning the parameters and the data generated by the model using the tuned parameters.

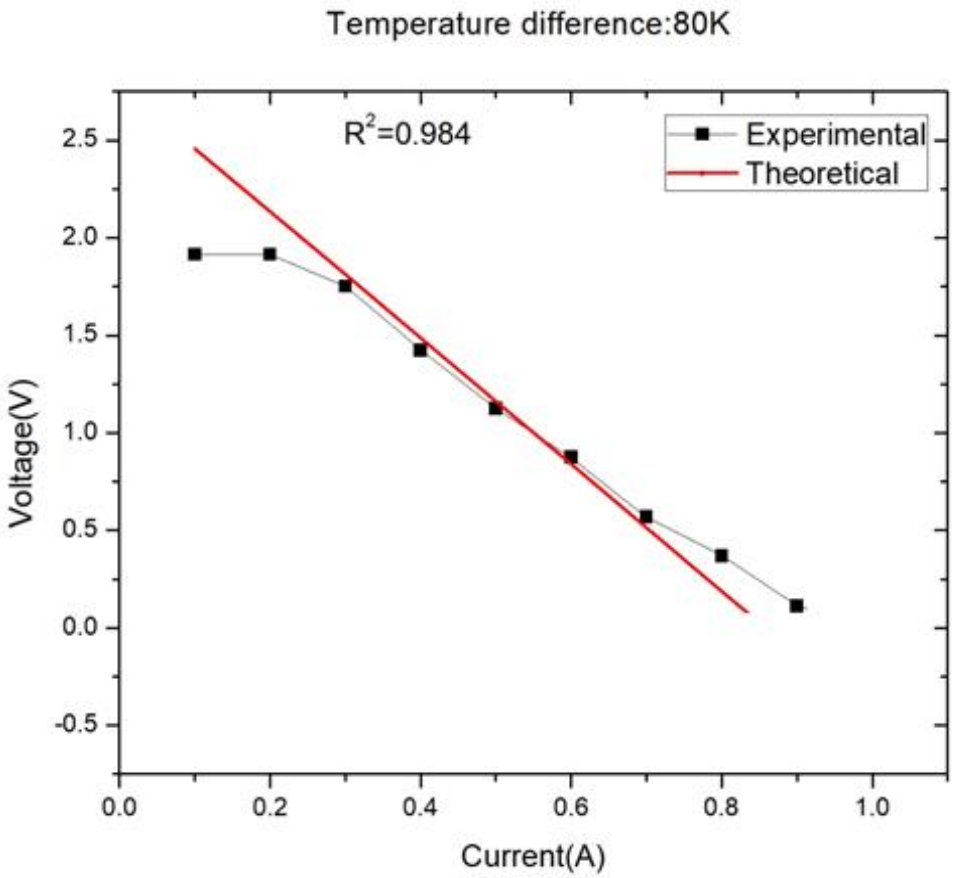

Fig 4.6 Voltage vs Current plot for the commercial thermoelectric generator, at 80K temperature difference

It is seen that the data generated from the tuned model agrees closely with the experimental data with an R^2 value of 0.984.

4.5 Case Study III: Validation of the tuned model formed in Case Study II against temperature differences of 100K, 120K and 140K.

Process Diagram

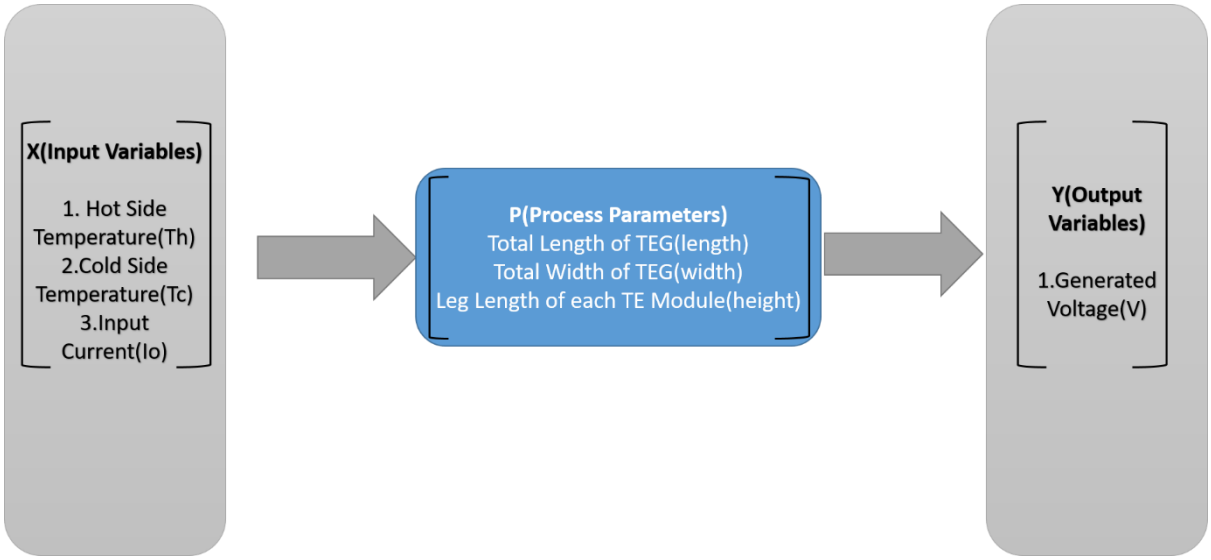

Fig 4.7 Process diagram of the thermoelectric generator, in which the input variables, output variables and the process parameters have been defined.

In this case study, the input variables (X) and the process parameters are known. However, the value of the output variables (Y) are unknown and are found out in this study.

4.5.1 Model Equations

Model equations are as shown in section 4.1. As in the previous case, the equations are solved simultaneously for each domain (I, II and III) for the thermoelectric generator shown in Fig 4.8 in COMSOL 5.3. Here in the figure below, Domain I and III consists of the Cu connectors, while Domain II consists of the P-type and N-type legs. COMSOL uses the finite element method to solve the coupled heat equations and electric potential equations.

4.5.2 Geometry

The geometry is formed from the tuned parameters shown below:

Table 4.5

Parameter name	Parameter Value	Description
width	25.4[mm]	Total width
length	25.4[mm]	Total length
height	1.9075[mm]	Leg Height

The COMSOL geometry is shown below:

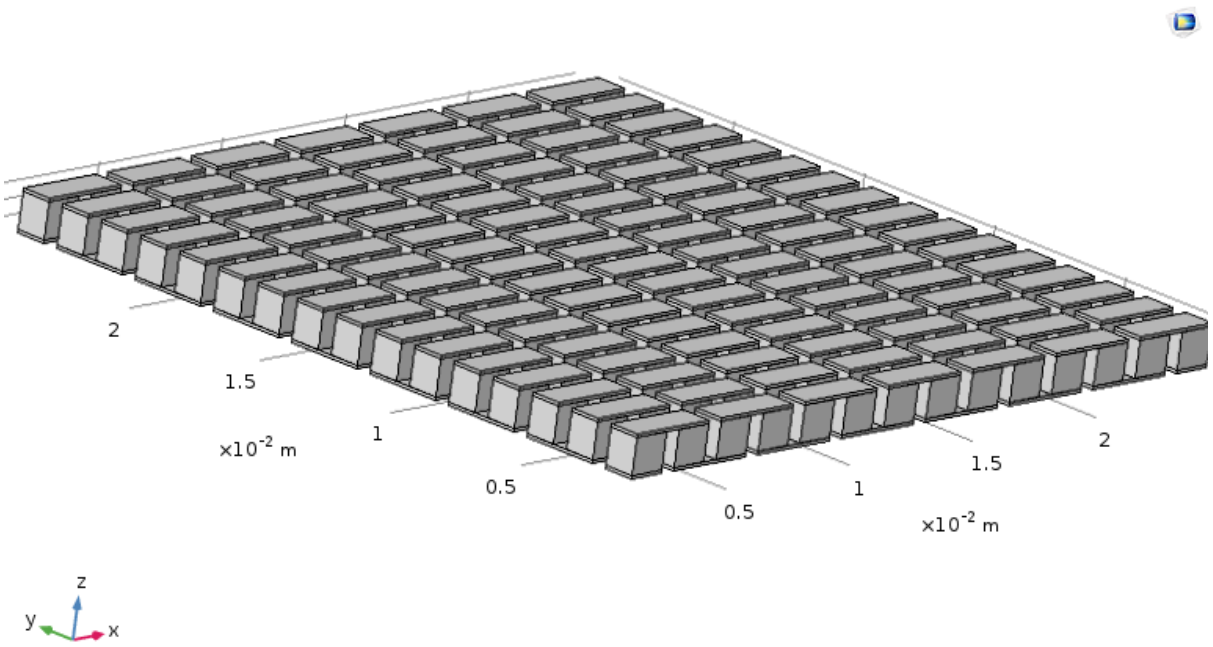

Fig 4.8 COMSOL model of the thermoelectric generator

4.5.3 Boundary conditions

Cold Side temperature of 293.15K

Hot Side Temperature of 373.15K (80K temperature difference), 393.15K (120K temperature difference), and 413.15K (140K temperature difference)

Input Current varying from 0.1A to 1.3

4.5.4 Results and Discussion

4.5.4.1 Temperature difference: 100K

At a temperature difference of 100K, the following data was obtained:

Table 4.6

Current (A)	Experimental Voltage(V)	Predicted Voltage(V)
0.1	2.725	3.14
0.2	2.725	2.8665
0.3	2.456	2.5623
0.4	2.135	2.2578
0.5	1.879	1.9528

0.6	1.526	1.6475
0.7	1.236	1.3417
0.8	0.952	1.0353
0.9	0.589	0.72846
1	0.365	0.42101
1.1	0	0.11294

The current voltage characteristics of the TEG are plotted (voltage plotted against current) and a comparison is made between the experimental data at 100K temperature difference and the data generated by the model using the tuned parameters, now at a temperature difference of 100K

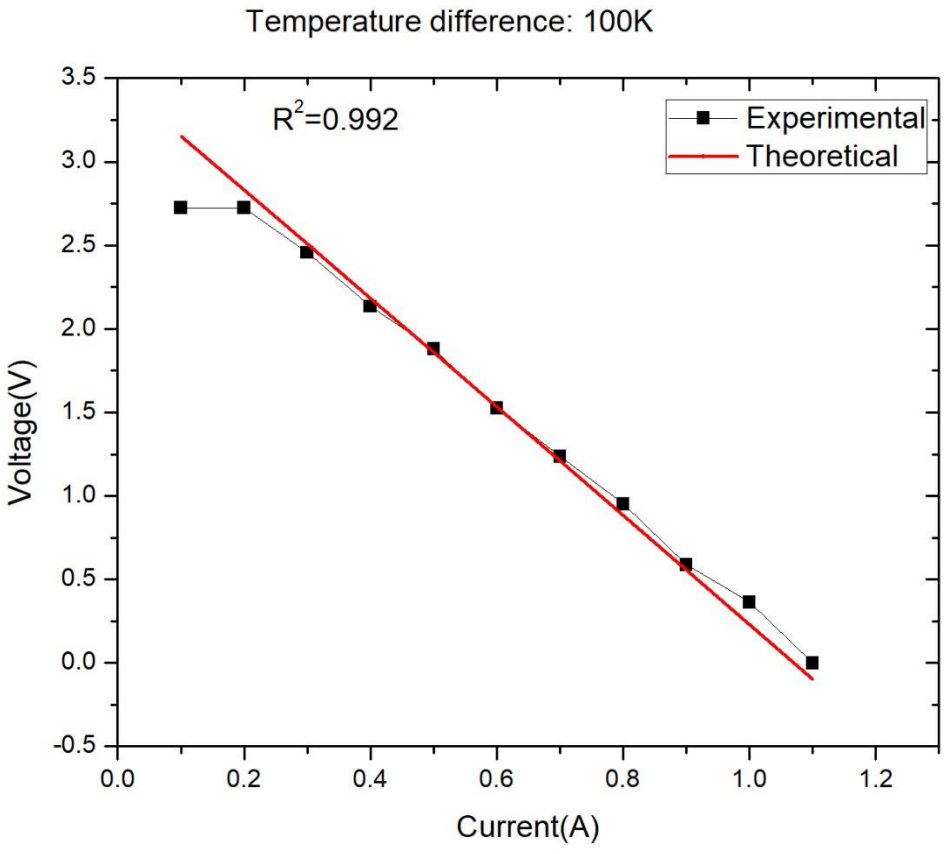

Fig 4.9 Voltage vs Current plot for the commercial thermoelectric generator, at 100K temperature difference

It is seen that the data generated from the tuned model, now at 100K temperature difference, agrees closely with the experimental data with an R^2 value of 0.992.

4.5.4.2 Temperature difference: 120K

At a temperature difference of 120K, the following data was obtained:

Table 4.7

Current (A)	Experimental Voltage(V)	Predicted Voltage(V)
0.1	4.055	3.9137
0.2	3.875	3.6159
0.3	3.569	3.3178
0.4	3.115	3.0193
0.5	2.785	2.7205
0.6	2.265	2.4212
0.7	1.874	2.1215
0.8	1.452	1.8213
0.9	1.023	1.5206
1	0.756	1.2192
1.1	0.412	0.91728
1.2	0	0.61468

The current voltage characteristics of the TEG are plotted (voltage plotted against current) and a comparison is made between the experimental data at 120K temperature difference and the data generated by the model using the tuned parameters, now at a temperature difference of 120K

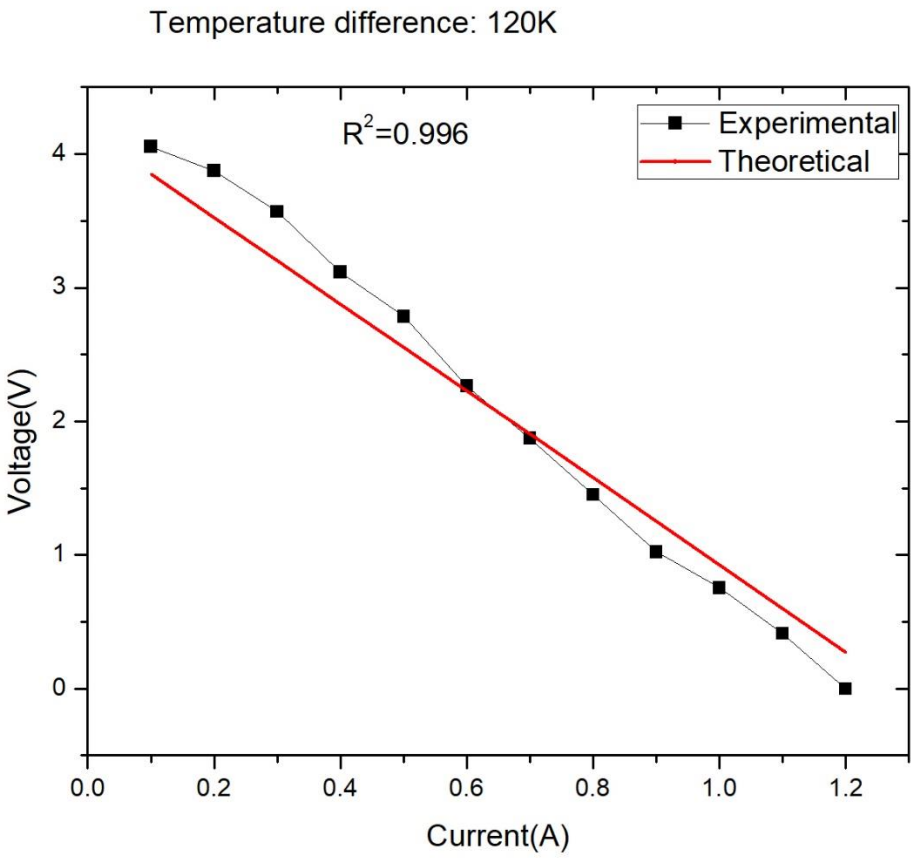

Fig 4.10 Voltage vs Current plot for the commercial thermoelectric generator, at 120K temperature difference

It is seen that the data generated from the tuned model, now at 120K temperature difference, agrees closely with the experimental data with an R^2 value of 0.996.

4.5.4.3 Temperature difference: 140K

At a temperature difference of 140K, the following data was obtained:

Table 4.8

Current (A)	Experimental Voltage(V)	Predicted Voltage(V)
0.1	4.199	4.5427
0.2	3.725	4.2198
0.3	3.654	3.8965
0.4	3.215	3.5729
0.5	2.7	3.2488
0.6	2.367	2.9243
0.7	1.987	2.5994
0.8	1.625	2.274
0.9	1.198	1.9483
1	0.865	1.6221
1.1	0.536	1.2955
1.2	0.201	0.96855
1.3	0	0.64115

The current voltage characteristics of the TEG are plotted (voltage plotted against current) and a comparison is made between the experimental data at 140K temperature difference and the data generated by the model using the tuned parameters, now at a temperature difference of 140K

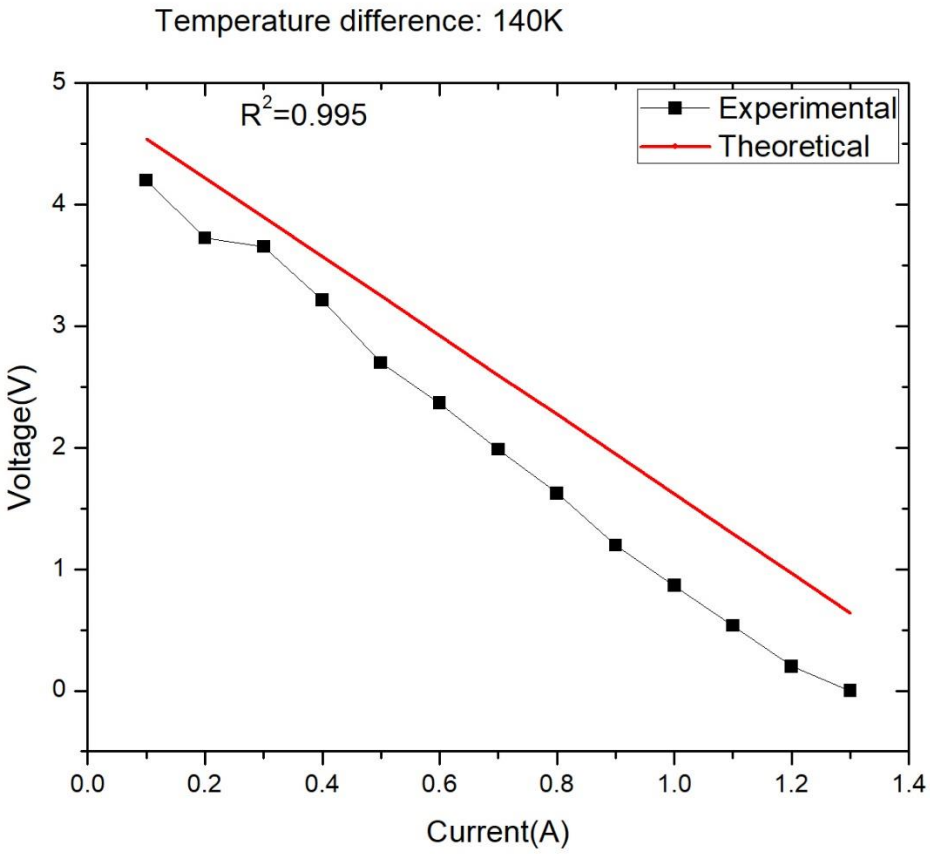

Fig 4.11 Voltage vs Current plot for the commercial thermoelectric generator, at 140K temperature difference

It is seen that the data generated from the tuned model, now at 140K temperature difference, agrees closely with the experimental data with an R^2 value of 0.995.

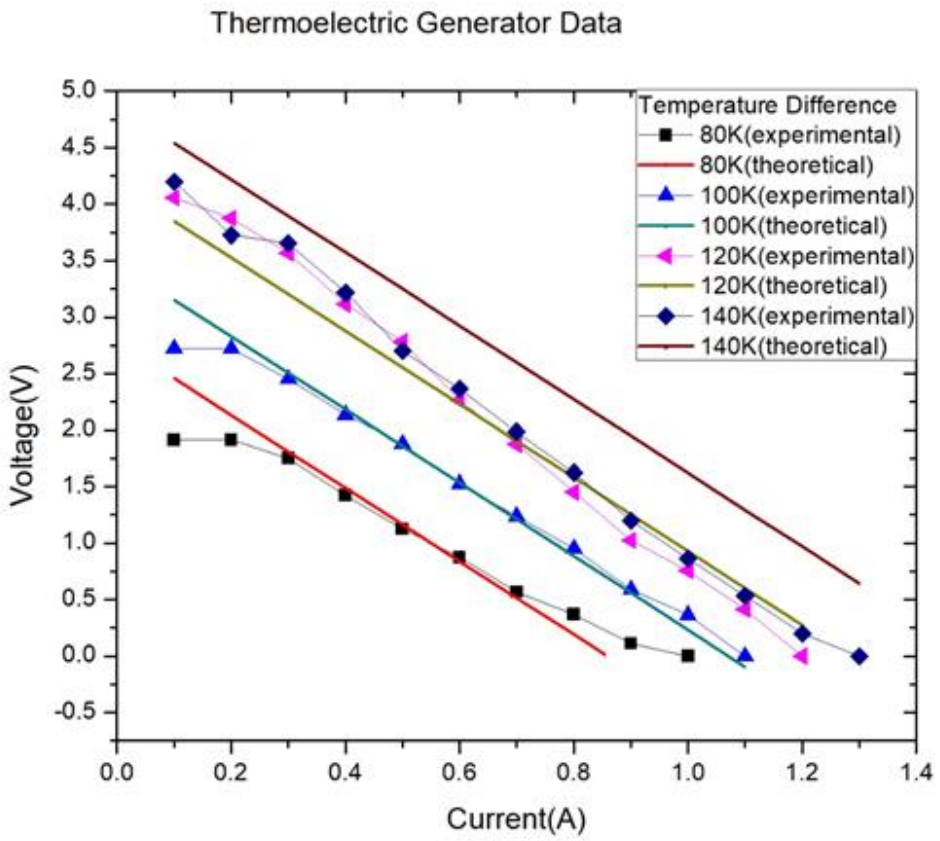

Fig 4.12 Consolidated Thermoelectric Generator Performance Curves

The experimental and model generated data are shown in the figure 4.12. It contains the sets of curves at all the temperature differences that have been evaluated in the study.

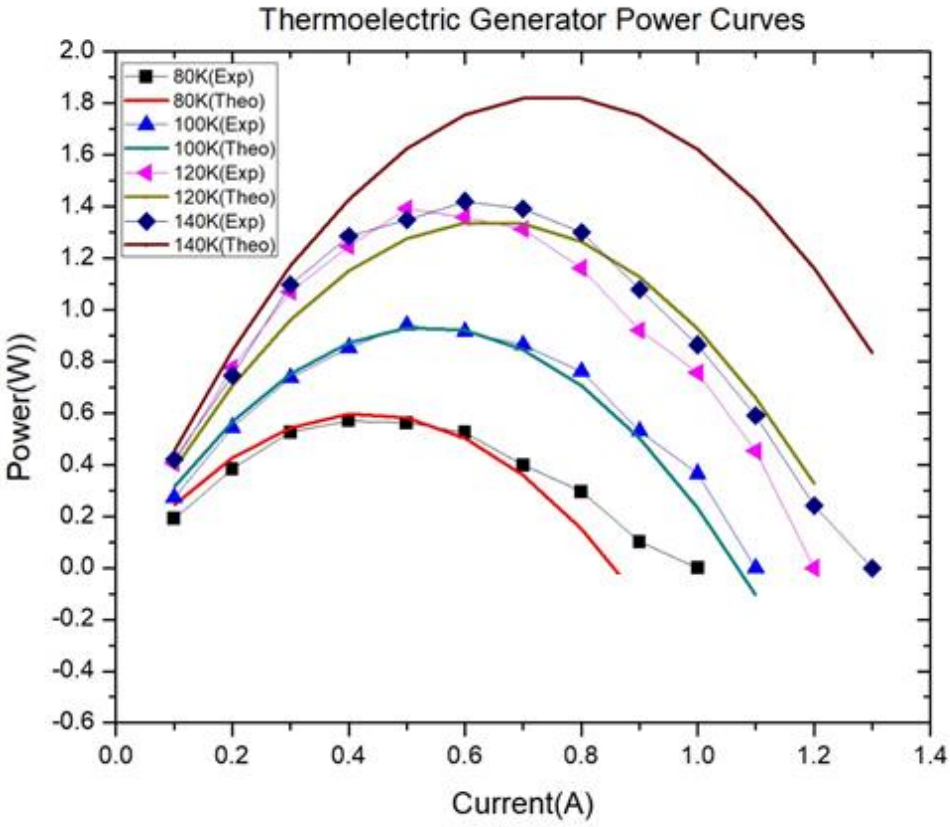

Fig 4.13 Consolidated Thermoelectric Generator Power Curves

The experimental and model generated data are shown in the figure 4.13. It contains the sets of power curves of the TEG at all the temperature differences that have been evaluated in the study.

CHAPTER-V

Tuning of COMSOL in-built fuel cell model

5.1 Fuel Cell Modeling

5.2 Description of variables solved for

Φs- Electronic potential

Φl- Ionic Potential

wH2—Hydrogen mass fraction (anode)

wH2Oa—Water mass fraction (anode)

wO2—Oxygen mass fraction (cathode)

wH2Oc—Water mass fraction (cathode)

wN2—Nitrogen mass fraction (cathode)

ua and uc —Velocity field vectors in the anode and cathode compartments

pa and pc —Pressure in the anode and cathode compartments

5.3 Physics and Multiphysics Couplings

Two Reacting Flow in Porous Media, Concentrated Species interfaces are coupled to one Secondary Current Distribution interface.

The Secondary Current Distribution interface is used to model the electrochemical currents.

Electrochemical Heat Dissipation multiphysics coupling is added to model the heat generation due to electrochemical reaction.

5.4 Electrode Reactions and Kinetics

On the anode, hydrogen oxidation occurs according to

$$H_2 => 2H^+ + 2e^- \quad (5.1)$$

The anode reaction is considered to be at equilibrium, due to fast kinetics.

At the cathode, oxygen reacts together with the protons to form water according to

$$O_2 + 4H^+ + 4e^- => 2H_2O$$

Butler Volmer Kinetics is used to represent the cathode kinetics.

$$\mathrm{i} = i_o(\exp\left(\frac{\alpha_a F\eta}{RT}\right) - \exp\left(\frac{\alpha_c F\eta}{RT}\right))$$

where i_o=1[A/m^2]*c_wO2/cO2_ref

$\alpha_a = 0.5$ and $\alpha_c = 0.9$

5.5 Mass transfer

wH2, wH2Oa, wO2, wH2Oc, and wH2Oc are solved for in the flow channels, GDLs and porous electrode using in the Maxwell-Stefan equations in two different Transport of Concentrated Species interfaces. One interface is used for each electrode compartment; hydrogen and water species are present on the anode whereas oxygen, water and nitrogen are present on the anode.

Couplings are made to the Secondary Current Distribution interface for the mass sources and sinks.

At the channel inlets the mass fractions are specified, and outflow conditions are used at the channel outlets. All other external boundaries use zero flux conditions.

5.6 Momentum transfer

u and p are modeled by the Navier-Stokes equations in the flow channels and the Brinkman equations for the porous gas diffusion layers (GDLs) and electrodes, using the Brinkman Equations interface.

Couplings for the density, velocity, pressure and net mass sources and sinks are made to the Transport of Concentrated Species interfaces by using Reacting Flow multiphysics nodes.

At the flow channel inlet boundaries, laminar inlet flow velocity profiles are specified, whereas a pressure is specified at the flow channel outlet boundaries. To model a multiple parallel channel configuration, symmetry boundary conditions are applied along the long sides of the GDLs and the porous electrodes. All other wall boundaries use no slip conditions.

5.7 Results

The model parameters are tuned (Identification problem) to match with the experimental data generated by experimental group of Polymer Engineering Laboratory, Chemical Engineering Department, Jadavpur University. The parameters are tuned and the equilibrium potential at each temperature obtained for which the model prediction match closely with the experimental data

5.7.1 Fuel Cell temperature: 100^0C

At a temperature of 100^0C the following data for the fuel cell was obtained:

Table 5.1

Current Density (A/cm^2)	**Power Density(W/cm^2) Experimental**	**Power Density(W/cm^2) Theoretical**
0	0	0
0.03333	0.025797	0.029985
0.06667	0.048802	0.055506
0.1	0.0714	0.078001
0.13333	0.091331	0.09882
0.16667	0.110752	0.117055
0.2	0.1291	0.134714
0.23333	0.143965	0.150605
0.26667	0.159202	0.164626
0.3	0.1734	0.177221
0.33333	0.188665	0.18885
0.36667	0.200202	0.19887
0.4	0.2112	0.207275
0.43333	0.222732	0.214235
0.46667	0.232868	0.220155
0.5	0.2425	0.224564
0.53333	0.246932	0.227465
0.56667	0.249901	0.228857
0.6	0.252	0.229004
0.63333	0.250799	0.227729
0.66667	0.249001	0.22498

0.7	0.2471	0.220759
0.73333	0.241999	0.214989
0.76667	0.236901	0.207559
0.8	0.2236	0.198635
0.83333	0.209999	0.188216
0.86667	0.190667	0.176297
0.9	0.1737	0.161923
0.93333	0.151199	0.145803
0.96667	0.116967	0.128097
1	0.089	0.108816
1.03333	0.059933	0.086567
1.06667	0.0288	0.061792

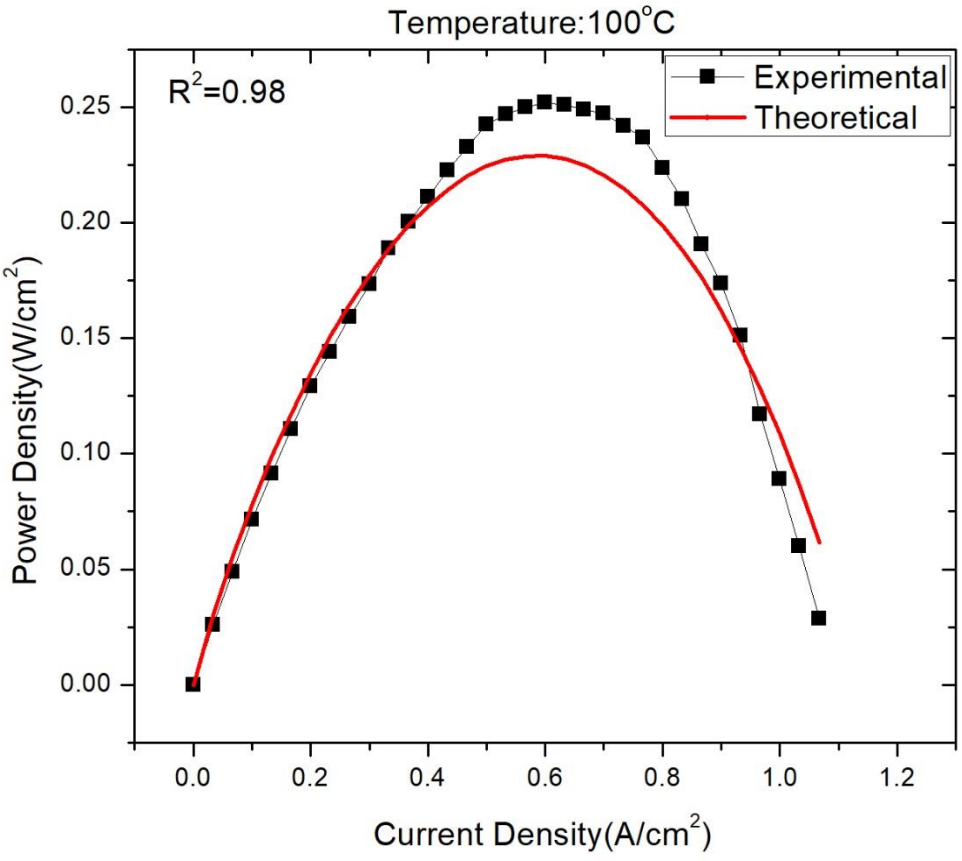

Fig 5.1 Power Density vs Current Density plot for fuel cell, at 100ºC temperature

It is seen that the data generated from the COMSOL fuel cell model at a temperature of 100^{o}C, agrees closely with the experimental data with an R^2 value of 0.98

5.7.2 Fuel Cell temperature: 120^{0}C

At a temperature of 120^{0}C the following data for the fuel cell was obtained:

Table 5.2

Current Density (A/cm^2)	Power Density(W/cm^2) Experimental	Power Density(W/cm^2) Theoretical
0	0	0
0.03333	0.027153	0.032559
0.06667	0.05186	0.059698
0.1	0.075729	0.084811
0.13333	0.097755	0.10677
0.16667	0.119319	0.128129
0.2	0.13915	0.147399
0.23333	0.157099	0.164552
0.26667	0.174456	0.180916
0.3	0.189888	0.195783
0.33333	0.206428	0.208929
0.36667	0.220416	0.220357
0.4	0.231956	0.230955
0.43333	0.243956	0.240019
0.46667	0.255002	0.247519
0.5	0.26504	0.25345
0.53333	0.27363	0.258161
0.56667	0.278025	0.261503
0.6	0.281766	0.263339
0.63333	0.282199	0.26367
0.66667	0.282388	0.262518
0.7	0.281505	0.259925
0.73333	0.27758	0.255836
0.76667	0.273441	0.250247
0.8	0.265016	0.243164

0.83333	0.254716	0.23408
0.86667	0.240735	0.223345
0.9	0.226152	0.211066
0.93333	0.203727	0.197243
0.96667	0.17548	0.181078
1	0.15289	0.162537
1.03333	0.129146	0.142344
1.06667	0.10448	0.120492
1.1	0.072721	0.095838
1.13333	0.0272	0.068156

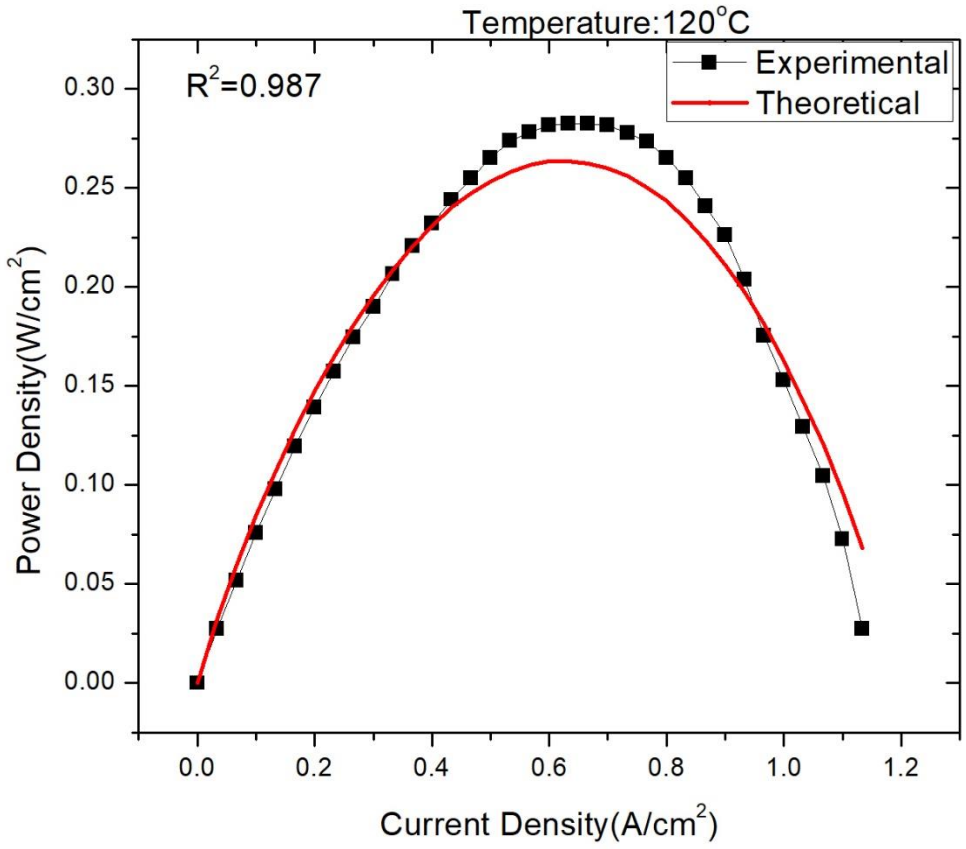

Fig 5.2 Power Density vs Current Density plot for fuel cell, at 120°C temperature

It is seen that the data generated from the COMSOL fuel cell model at a temperature of 120°C, agrees closely with the experimental data with an R^2 value of 0.987.

5.7.3 Fuel Cell temperature: 140^0C

At a temperature of 140^0C the following data for the fuel cell was obtained:

Table 5.3

Current Density (A/cm^2)	Power Density(W/cm^2) Experimental	Power Density(W/cm^2) Theoretical
0	0	0
0.03333	0.027618	0.034445
0.06667	0.053068	0.065245
0.1	0.077634	0.092383
0.13333	0.100277	0.117332
0.16667	0.122677	0.140775
0.2	0.143198	0.161853
0.23333	0.1616	0.181928
0.26667	0.180109	0.200588
0.3	0.196776	0.217408
0.33333	0.214021	0.232502
0.36667	0.228028	0.246816
0.4	0.241064	0.259501
0.43333	0.254131	0.270561
0.46667	0.266464	0.279999
0.5	0.277705	0.288441
0.53333	0.287129	0.295343
0.56667	0.293184	0.300706
0.6	0.298638	0.304526
0.63333	0.301091	0.306976
0.66667	0.303608	0.307988
0.7	0.304269	0.307487
0.73333	0.303254	0.305471
0.76667	0.302114	0.301866
0.8	0.296424	0.296534
0.83333	0.289016	0.289664
0.86667	0.277811	0.281254
0.9	0.267804	0.271308
0.93333	0.249488	0.25877

0.96667	0.224809	0.24454
1	0.20403	0.228696
1.03333	0.181577	0.211234
1.06667	0.158571	0.19052
1.1	0.132242	0.167718
1.13333	0.100866	0.143173
1.16667	0.051333	0.116877
1.2	0.006	0.08631

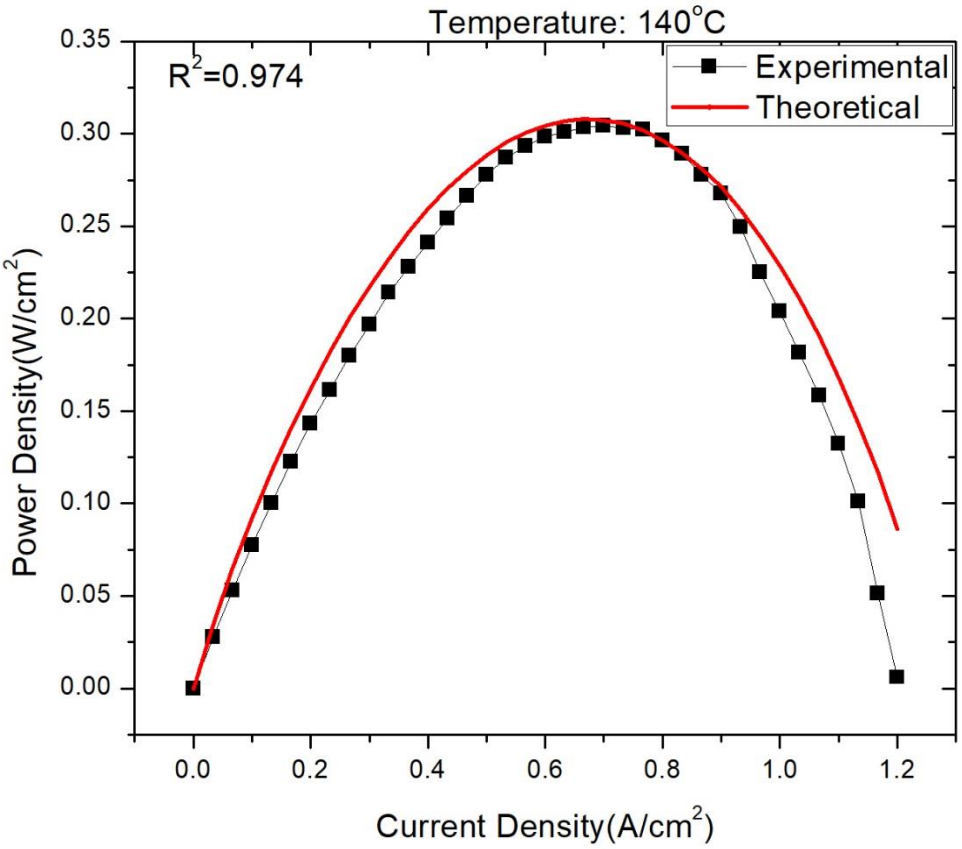

Fig 5.4 Power Density vs Current Density plot for fuel cell, at 140ºC temperature

It is seen that the data generated from the COMSOL fuel cell model at a temperature of 140ºC, agrees closely with the experimental data with an R^2 value of 0.974.

5.7.4 Fuel Cell temperature: 160^0C

At a temperature of 160^0C the following data for the fuel cell was obtained:

Table 5.4

Current Density (A/cm^2)	Power Density(W/cm^2) Experimental	Power Density(W/cm^2) Theoretical
0	0	0
0.03333	0.027658	0.036531
0.06667	0.053334	0.070738
0.1	0.078328	0.102599
0.13333	0.101927	0.132125
0.16667	0.125429	0.159324
0.2	0.147432	0.18418
0.23333	0.1681	0.207395
0.26667	0.188677	0.229651
0.3	0.208068	0.250057
0.33333	0.227861	0.26862
0.36667	0.245464	0.286217
0.4	0.262588	0.30238
0.43333	0.279186	0.316901
0.46667	0.29536	0.329784
0.5	0.31061	0.341469
0.53333	0.324883	0.351751
0.56667	0.33646	0.360476
0.6	0.347682	0.367637
0.63333	0.355539	0.37335
0.66667	0.365588	0.377654
0.7	0.371686	0.380422
0.73333	0.377944	0.381656
0.76667	0.382377	0.381328
0.8	0.384696	0.37924
0.83333	0.386323	0.375596
0.86667	0.383553	0.370396
0.9	0.382275	0.363642
0.93333	0.376365	0.354483

0.96667	0.366126	0.343521
1	0.35688	0.330934
1.03333	0.346806	0.316718
1.06667	0.335862	0.299481
1.1	0.322916	0.280016
1.13333	0.305999	0.258804
1.16667	0.283501	0.235838
1.2	0.2484	0.209013
1.23333	0.215833	0.180129
1.26667	0.172267	0.14936
1.3	0.1287	0.115816
1.33333	0.082666	0.078713
1.36667	0.017767	0.039595

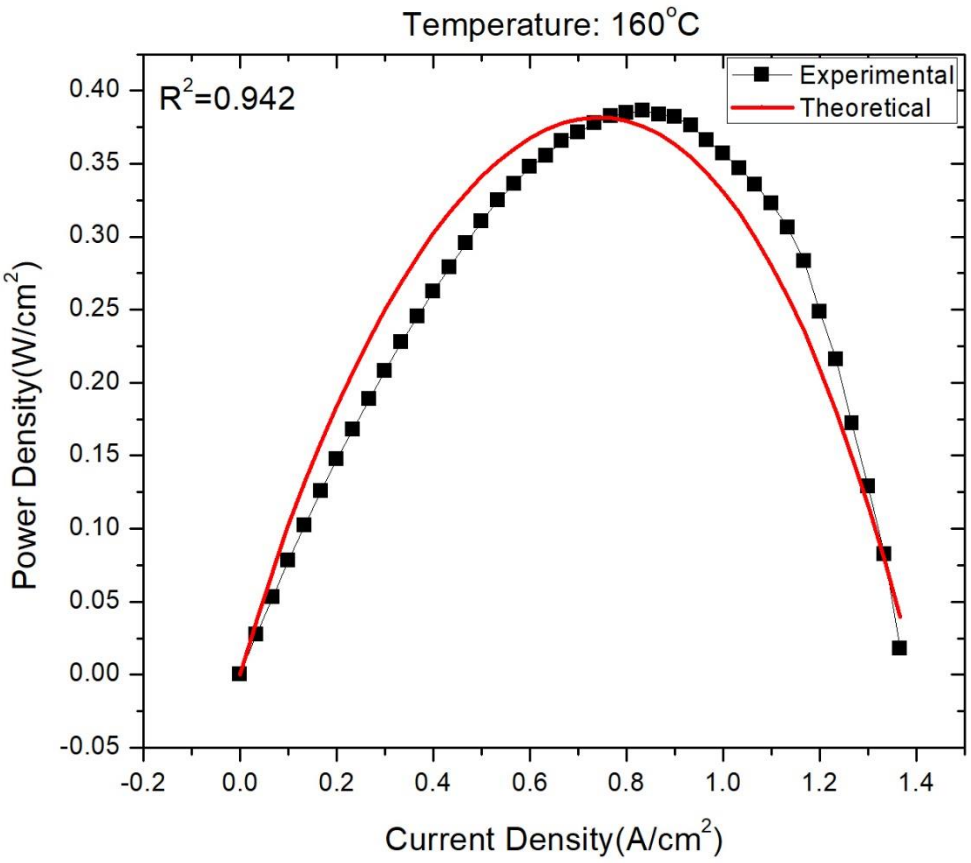

Fig 5.5 Power Density vs Current Density plot for fuel cell, at 160ºC temperature

It is seen that the data generated from the COMSOL fuel cell model at a temperature of 160°C, agrees closely with the experimental data with an R^2 value of 0.942.

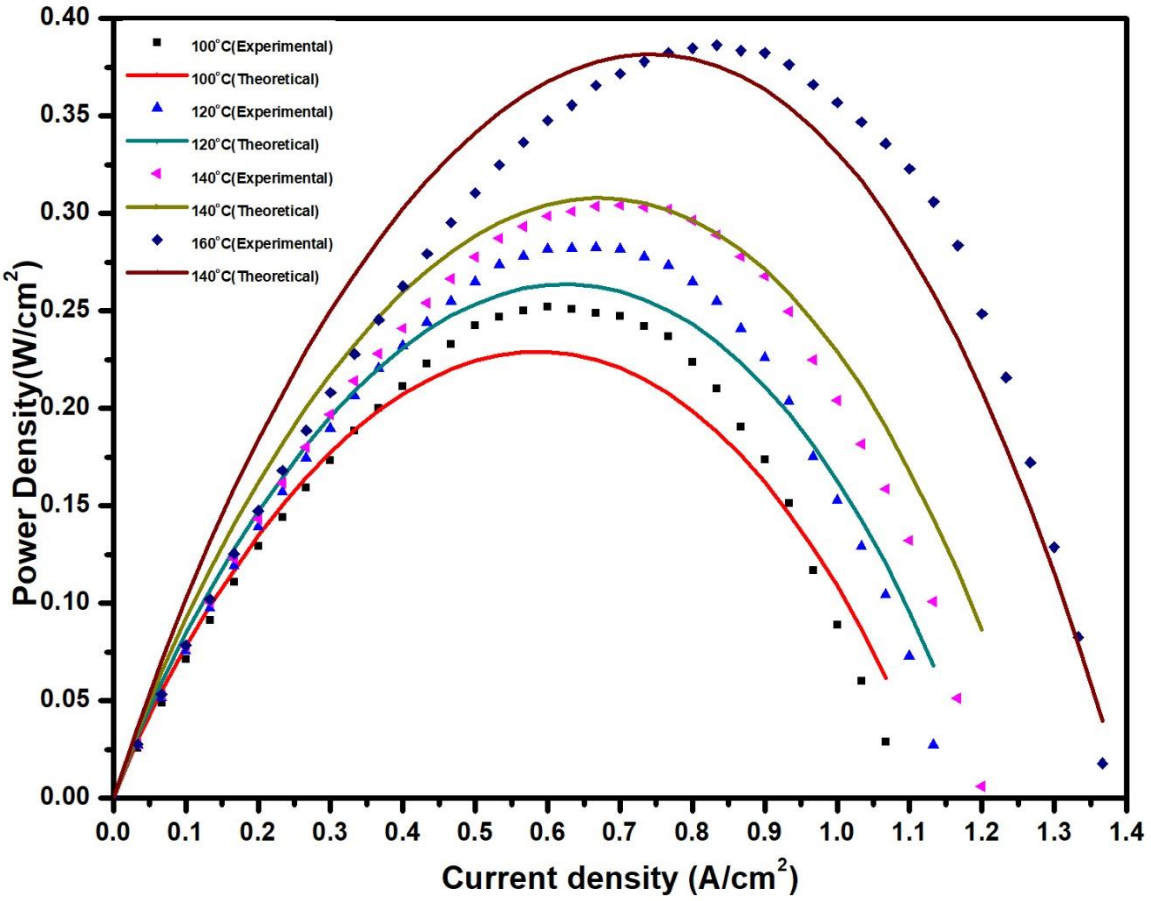

Fig 5.6 Consolidated Power Density Curves for Fuel Cell

CHAPTER-VI

Modeling of FC-TEG Hybrid

6.1 Diagram of the FC-TEG hybrid

The fuel cell and the thermoelectric generator are combined to produce a hybrid FC-TEG. There is a heater input to maintain the temperature. The objective of the hybrid modelling is to predict the window of voltage for which hybrid FC-TEG can operate with a net power output.

For each operating temperature, there exists a threshold voltage below which the overall process is feasible.

whose diagram is shown as follows:

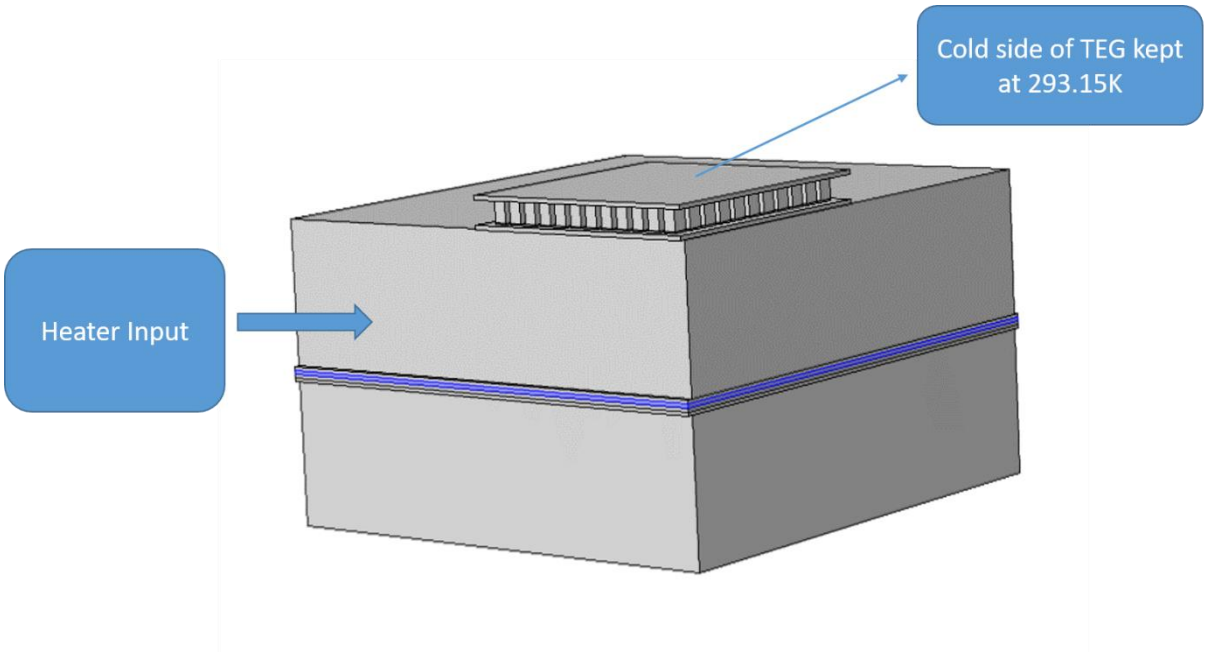

Fig 6.1 COMSOL Model of the hybrid FC-TEG

6.2 Model equations

The following equations are solved within the fuel cell boundary

$$\nabla.(k\nabla T) + Q_h = 0 \qquad (6.1)$$

Where Q_h takes into consideration the joule heating losses and overpotential losses, which give rise to heat generation within the fuel cell. This is implemented by the electrochemical heat source multiphysics coupling in COMSOL.

$$Q_h = Q_{JH} + \sum a_{v,m} Q_m$$

$$Q_{JH} = -(i_s \nabla \emptyset_s + i_l \nabla \emptyset_l)$$

$$Q_m = (\emptyset_s - \emptyset_l - E_{eq,m}) i_{loc,m}$$

Where Q_{JH} denotes the Joule heating losses and Q_m denotes the overpotential losses.

Across the boundary of the fuel cell and the thermoelectric generator, the heat flux is continuous.

The thermoelectric generator is modelled with the equations given in section 4.1.

6.3 Boundary conditions

All boundaries of the fuel cell are insulated except one face at which a constant heat rate of Qo watts is supplied, in order to model the heater.

All boundaries of the thermoelectric generator are insulated except the cold side of the thermoelectric generator, which is maintained at a temperature of 293.15K,

6.4 Simulation studies on the FC-TEG hybrid

A heater has been added, and a study has been performed in which the heater power required to maintain the fuel cell temperatures has been found out. This is followed by plots of net power output versus fuel cell temperature at different fuel cell voltages.

6.5 Results

At a fuel cell temperature of 100°C, the following data were found out:

Table 6.1

Fuel cell Voltage(V)	Fuel cell Current Density(A/cm²)	Heater Input (W)	Fuel Cell Power(W)	Fuel Cell Power-Heater Input(W)
0	1.1104	-2.52	0	2.52
0.1	0.96095	0	0.38438	0.38438
0.2	0.85318	2.7	0.682544	-2.017456
0.3	0.73025	5.45	0.8763	-4.5737
0.4	0.59727	8.093	0.955632	-7.137368
0.5	0.46137	10	0.92274	-9.07726
0.6	0.32718	11.923	0.785232	-11.137768
0.7	0.2043	13.2569	0.57204	-12.68486
0.8	0.10572	14.15	0.338304	-13.811696
0.9	0.047745	14.977	0.171882	-14.805118
1	0.017572	14.977	0.070288	-14.906712

At a fuel cell temperature of 120°C, the following data were found out:

Table 6.2

Voltage(V)	Current Density(A/cm2)	Heater Input (W)	Fuel Cell Power(W)	Fuel Cell Power-Heater Input(W)
0	1.2076	-2	0	2
0.1	1.077	1.492	0.4308	-1.0612
0.2	0.92837	4.7	0.742696	-3.957304
0.3	0.78214	7.7375	0.938568	-6.798932
0.4	0.63479	10.51	1.015664	-9.494336
0.5	0.48783	13.1	0.97566	-12.12434
0.6	0.34824	15.15	0.835776	-14.314224
0.7	0.22101	16.85	0.618828	-16.231172
0.8	0.12016	17.95625	0.384512	-17.571738
0.9	0.056453	18.49375	0.2032308	-18.2905192
1	0.023128	18.7	0.092512	-18.607488

At a fuel cell temperature of 140°C, the following data were found out:

Table 6.3

Voltage(V)	Current Density(A/cm2)	Heater Input (W)	Fuel Cell Power(W)	Fuel Cell Power-Heater Input(W)
0	1.27	0	0	0
0.1	1.14	3.286	0.456	-2.83
0.2	1	6.7	0.8	-5.9
0.3	0.85813	10	1.029756	-8.970244
0.4	0.70762	13	1.132192	-11.867808
0.5	0.56562	15.27	1.13124	-14.13876
0.6	0.42293	17.653	1.015032	-16.637968
0.7	0.28901	19.669	0.809228	-18.859772
0.8	0.17362	21.211	0.555584	-20.655416
0.9	0.089849	22.119	0.3234564	-21.7955436
1	0.042441	22.53	0.169764	-22.360236

At a fuel cell temperature of 160^{o}C, the following data were found out:

Table 6.4

Voltage(V)	Current Density(A/cm2)	Heater Input (W)	Fuel Cell Power(W)	Fuel Cell Power-Heater Input(W)
0	1.4157	-1.411	0	1.411
0.1	1.2868	2.52	0.51472	-2.00528
0.2	1.1611	6.196	0.92888	-5.26712
0.3	1.0215	9.8	1.2258	-8.5742
0.4	0.8782	12.9	1.40512	-11.49488
0.5	0.72928	15.67	1.45856	-14.21144
0.6	0.58359	18.5	1.400616	-17.099384
0.7	0.4405	21.1	1.2334	-19.8666
0.8	0.30803	23.06	0.985696	-22.074304
0.9	0.19166	24.687	0.689976	-23.997024
1	0.10401	25.749	0.41604	-25.33296

The net power output (thermoelectric power plus fuel cell power minus heater input) of the fuel cell at different voltages is plotted against temperature in the following graph.

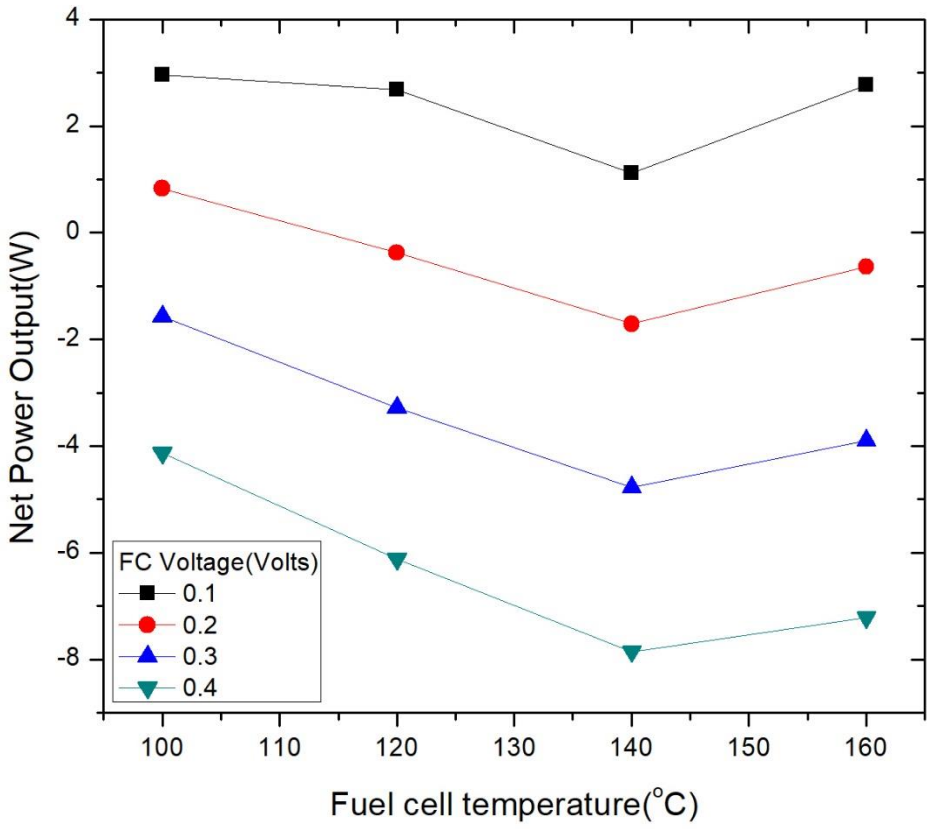

Fig 6.2 Net Power Output vs Fuel cell temperature for different values of fuel cell voltages

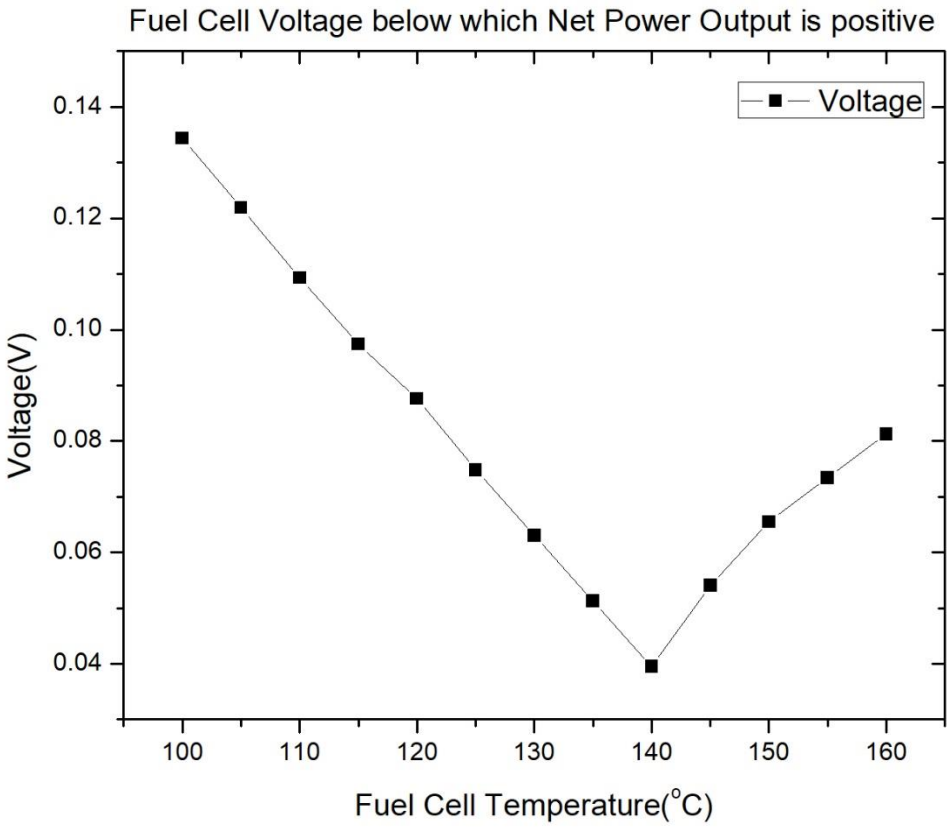

Fig 6.3 Fuel cell Voltage at which Net Power Output becomes zero. For a particular value of fuel cell temperature, the voltage on the graph signifies the voltage below which the net power output becomes zero.

CHAPTER-VII

Conclusion

7.1 Conclusion

1. A COMSOL Model has been developed for a single TEG and validated with experimental data in literature.

2. Model of the TEG comprises of 112 thermoelectric elements developed using COMSOL and is validated with experimental data.

3. The inbuilt fuel cell model in COMSOL is tuned to match with experimental data generated by the experimental group of Polymer Engineering Laboratory, Chemical Engineering Department, Jadavpur University.

4. A hybrid fuel cell-thermoelectric generator(FC-TEG) model to check the feasibility and window of operating zone for the system has been developed in COMSOL.

5. The threshold voltage vs temperature plot has been generated for the hybrid FC-TEG.

6. Significance of this study is in power generation for remote applications.

References

[1] T. Wang, et al., **Waste heat recovery through plate heat exchanger based thermoelectric generator system** Appl Energy, 136 (2014), pp. 860-865

[2] Ovik R. Fitriani, B.D. Long, M.C. Barma, M. Riaz, M.F.M. Sabri, S.M. Said, R. Saidur, A **review on nanostructures of high-temperature thermoelectric materials for waste heat recovery** Renew. Sustain. Energy Rev., 64 (2016), pp. 635-659

[3] Marit Takla, Odne Burheim, Leiv Kolbeinsen, Signe Kjelstrup, A **Solid State Thermoelectric Power Generator Prototype Designed to Recover Radiant Waste Heat** Carbon Dioxide Management and Other Technologies, 2012

[4] Yan Chen, Xiangnan Hou, Chunyan Ma, Yinke Dou, and Wentao Wu, **Review of Development Status of Bi2Te3-Based Semiconductor Thermoelectric Power Generation**, Advances in Materials Science and Engineering, 2018

[5] Xiao-Dong Wang Yu-Xian Huang, Chin-Hsiang Cheng, David Ta-Wei Lin, Chung-Hao Kang, **A three-dimensional numerical modeling of thermoelectric device with consideration of coupling of temperature field and electric potential field,** Energy 47 (2012) 488-497

[6] S. Manikandan , S.C. Kaushik, **Energy and exergy analysis of an annular thermoelectric cooler,** Energy Conversion and Management 106 (2015) 804–814

[7] Jing-Hui Meng , Xin-Xin Zhang , Xiao-Dong Wang, **Characteristics analysis and parametric study of a thermoelectric generator by considering variable material properties and heat losses**, International Journal of Heat and Mass Transfer 80 (2015) 227–235

[8] P. Aranguren , M. Araiz, D. Astrain, A. Martínez, **Thermoelectric generators for waste heat harvesting: A computational and experimental approach**, Energy Conversion and Management 148 (2017) 680–691

[9] D. Astrain, J.G. Vian, A. Martınez, A. Rodrıguez, **Study of the influence of heat exchangers' thermal resistances on a thermoelectric generation system**, Energy 35 (2010) 602–610

[10] Byung deok In, Hyung ik Kim, Jung wook Son, Ki hyung Lee b, **The study of a thermoelectric generator with various thermal conditions of exhaust gas from a diesel engine**, International Journal of Heat and Mass Transfer 86 (2015) 667–680

[11] Hsiao-Kang Ma, Ching-Po Lin, How-Ping Wu, Chun-Hao Peng, Chia-Cheng Hsu, **Waste heat recovery using a thermoelectric power generation system in a biomass gasifier**, Applied Thermal Engineering 88 (2015) 274-279

[12] X. Chen, Y. Pan, J.Chen, **Performance and Evaluation of a Fuel Cell–Thermoelectric Generator Hybrid System**, FUEL CELLS 10, 2010, No. 6, 1164–1170

[13] Xin Gao, Søren Juhl Andreasen, Min Chen, Søren Knudsen Kær, **Numerical model of a thermoelectric generator with compact plate-fin heat exchanger for high temperature PEM fuel cell exhaust heat recovery**, International Journal of Hydrogen Energy Volume 37, Issue 10, May 2012, Pages 8490-8498

[14] Puqing Yang, Ying Zhua Pei Zhang, Houcheng Zhang, Ziyang Hua Jinjie Zhang, **Performance evaluation of an alkaline fuel cell/thermoelectric generator hybrid system**, International Journal of Hydrogen Energy Volume 39, Issue 22, 24 July 2014, Pages 11756-11762

[15] Hai-Peng Li, Rui-Qin Zhang, **Surface effects on the thermal conductivity of silicon nanowires,** Chin. Phys. B Vol. 27, No. 3 (2018)

[16] Hassan Abdullah Alzahrani, **Combining thermogalvanic corrosion and thermogalvanic redox couples for electrochemical waste heat harvesting**, Master Degree Thesis, The University of New South Wales.

[17] G. Jeffrey Snyder, Eric S. Toberer, **Complex Thermoelectric Materials**, Nature Materials 7, 105-114 (2008).

[18] N F A Abdul Rahman, N. F. Mohd Zambri, H. C. Mat Haris, M. H. Fazalul Rahiman, **Design and development of thermoelectric generator kit from car engine heat,** 2016 IEEE Conference on Systems, Process and Control